

REPORT DOCUMENTATION PAGE			Form Approved OMB NO. 0704-0188		
<p>The public reporting burden for this collection of information is estimated to average 1 hour per response, including the time for reviewing instructions, searching existing data sources, gathering and maintaining the data needed, and completing and reviewing the collection of information. Send comments regarding this burden estimate or any other aspect of this collection of information, including suggestions for reducing this burden, to Washington Headquarters Services, Directorate for Information Operations and Reports, 1215 Jefferson Davis Highway, Suite 1204, Arlington VA, 22202-4302. Respondents should be aware that notwithstanding any other provision of law, no person shall be subject to any penalty for failing to comply with a collection of information if it does not display a currently valid OMB control number.</p> <p>PLEASE DO NOT RETURN YOUR FORM TO THE ABOVE ADDRESS.</p>					
1. REPORT DATE (DD-MM-YYYY) 10-06-2010		2. REPORT TYPE Final Report		3. DATES COVERED (From - To) 17-May-2006 - 16-Nov-2009	
4. TITLE AND SUBTITLE Final Progress Report Fundamentals of Wireless Networks: Connectivity and Capacity ARO Grant W911NF-06-1-0182			5a. CONTRACT NUMBER W911NF-06-1-0182		
			5b. GRANT NUMBER		
			5c. PROGRAM ELEMENT NUMBER 611102		
6. AUTHORS Gerhard Kramer and Yuliy Baryshnikov			5d. PROJECT NUMBER		
			5e. TASK NUMBER		
			5f. WORK UNIT NUMBER		
7. PERFORMING ORGANIZATION NAMES AND ADDRESSES Lucent Technology 600 Mountain Avenue PO Box 636 Murray Hill, NJ 07974 -0636			8. PERFORMING ORGANIZATION REPORT NUMBER		
9. SPONSORING/MONITORING AGENCY NAME(S) AND ADDRESS(ES) U.S. Army Research Office P.O. Box 12211 Research Triangle Park, NC 27709-2211			10. SPONSOR/MONITOR'S ACRONYM(S) ARO		
			11. SPONSOR/MONITOR'S REPORT NUMBER(S) 49466-MA.1		
12. DISTRIBUTION AVAILABILITY STATEMENT Approved for Public Release; Distribution Unlimited					
13. SUPPLEMENTARY NOTES The views, opinions and/or findings contained in this report are those of the author(s) and should not be construed as an official Department of the Army position, policy or decision, unless so designated by other documentation.					
14. ABSTRACT This report reviews the scientific progress and accomplishments supported by ARO Grant W911NF-06-1-0182 : Fundamentals of Wireless Networks, Connectivity and Capacity					
15. SUBJECT TERMS virtual communication ad-hoc network, wireless nodes, cellular automata theory, wake-node pathways					
16. SECURITY CLASSIFICATION OF:			17. LIMITATION OF ABSTRACT UU	15. NUMBER OF PAGES	19a. NAME OF RESPONSIBLE PERSON Gerhard Kramer
a. REPORT UU	b. ABSTRACT UU	c. THIS PAGE UU			19b. TELEPHONE NUMBER 908-582-3964

Report Title

Final Progress Report
Fundamentals of Wireless Networks: Connectivity and Capacity
ARO Grant W911NF-06-1-0182

ABSTRACT

This report reviews the scientific progress and accomplishments supported by ARO Grant W911NF-06-1-0182 : Fundamentals of Wireless Networks, Connectivity and Capacity

List of papers submitted or published that acknowledge ARO support during this reporting period. List the papers, including journal references, in the following categories:

(a) Papers published in peer-reviewed journals (N/A for none)

I. Maric, A. Goldsmith, G. Kramer, S. Shamaï (Shitz), "On the capacity of interference channels with one cooperating transmitter," Eur. Trans. Telecommun., vol. 19, no. 4, pp. 405-420, June 2008. DOI: 10.1002/ett.1298

A. Sanderovich, S. Shamaï (Shitz), Y. Steinberg, G. Kramer, "Communication via decentralized processing," IEEE Trans. Inf. Theory, vol. 54, no. 7, pp. 3008-3023, July 2008.

X. Shang, G. Kramer, B. Chen, "A new outer bound and the noisy-interference sum-rate capacity for Gaussian interference channels," IEEE Trans. Inf. Theory, vol. 55, no. 2, pp. 689-699, Feb. 2009.

Y. Liang, G. Kramer, H. V. Poor, S. Shamaï (Shitz), "Compound wiretap channels," EURASIP J. Wireless Commun. Network., vol. 2009, Article ID 142374, 12 pages, DOI: 10.1155/2009/142374

Number of Papers published in peer-reviewed journals: 4.00

(b) Papers published in non-peer-reviewed journals or in conference proceedings (N/A for none)

Number of Papers published in non peer-reviewed journals: 0.00

(c) Presentations

G. Kramer, "Cooperative Communications and Compress-and-Forward", Institute for Infocomm Research Departmental Internal Workshop, Agency for Science, Technology and Research (A*STAR), Singapore, Singapore, July 2009.

G. Kramer, "Coding for Cooperation and Relaying with a Focus on "Compress-and-Forward"", Keynote Talk, RAWNET Workshop, Seoul, South Korea, June 2009.

G. Kramer, "Cooperative Communications and Compress-and-Forward", Plenary Talk, NEWCOM++ - ACoRN Joint Workshop, Barcelona, Spain, April 2009.

G. Kramer, "Coding for Cooperation and Relaying", 5th Int. Symp. Turbo Coding & Related Topics, Lausanne, Switzerland, Sept. 2008.

Number of Presentations: 4.00

Non Peer-Reviewed Conference Proceeding publications (other than abstracts):

Y. Liang, G. Kramer, H.V. Poor, S. Shamaï (Shitz), "Recent results on compound wire-tap channels," IEEE Int. Symp. Personal, Indoor, and Mobile Radio Commun. (PIMRC), Cannes, France, pp. 1-5, Sept. 15-18, 2008.

G. Kramer, "Communication on line networks with deterministic or erasure broadcast channels," 2009 IEEE Inf. Theory Workshop, Taormina, Italy, pp. 404-405, Oct. 11-16, 2009.

Y. Liang, G. Kramer, H. V. Poor, S. Shamaï (Shitz), "Compound wiretap channels," EURASIP J. Wireless Commun. Network., vol. 2009, Article ID 142374, 12 pages, DOI: 10.1155/2009/142374

Peer-Reviewed Conference Proceeding publications (other than abstracts):

Information Processing In Sensor Networks archive Proceedings of the 7th international conference on Information processing in sensor networks table of contents Pages: 517-526 Year of Publication: 2008

Self-assembling sweep-and-sleep sensor systems K. J. Kwak, Y. M. Baryshnikov, E. G. Coffman; August 2008
SIGMETRICS Performance Evaluation Review , Volume 36 Issue 2

Self-Organizing Sleep-Wake Sensor Systems Kyung Joon Kwak, Yuliy M. Baryshnikov, Edward G. Coffman; October 2008
SASO '08: Proceedings of the 2008 Second IEEE International Conference on Self-Adaptive and Self-Organizing Systems, Publisher: IEEE Computer Society

Number of Peer-Reviewed Conference Proceeding publications (other than abstracts):

3

(d) Manuscripts

Number of Manuscripts: 0.00

Patents Submitted**Patents Awarded****Graduate Students**

<u>NAME</u>	<u>PERCENT SUPPORTED</u>
FTE Equivalent:	
Total Number:	

Names of Post Doctorates

<u>NAME</u>	<u>PERCENT SUPPORTED</u>
FTE Equivalent:	
Total Number:	

Names of Faculty Supported

<u>NAME</u>	<u>PERCENT SUPPORTED</u>
FTE Equivalent:	
Total Number:	

Names of Under Graduate students supported

<u>NAME</u>	<u>PERCENT SUPPORTED</u>
FTE Equivalent:	
Total Number:	

Student Metrics

This section only applies to graduating undergraduates supported by this agreement in this reporting period

- The number of undergraduates funded by this agreement who graduated during this period: 0.00
- The number of undergraduates funded by this agreement who graduated during this period with a degree in science, mathematics, engineering, or technology fields:..... 0.00
- The number of undergraduates funded by your agreement who graduated during this period and will continue to pursue a graduate or Ph.D. degree in science, mathematics, engineering, or technology fields:..... 0.00
- Number of graduating undergraduates who achieved a 3.5 GPA to 4.0 (4.0 max scale):..... 0.00
- Number of graduating undergraduates funded by a DoD funded Center of Excellence grant for Education, Research and Engineering:..... 0.00
- The number of undergraduates funded by your agreement who graduated during this period and intend to work for the Department of Defense 0.00
- The number of undergraduates funded by your agreement who graduated during this period and will receive scholarships or fellowships for further studies in science, mathematics, engineering or technology fields: 0.00

Names of Personnel receiving masters degrees

<u>NAME</u>
Total Number:

Names of personnel receiving PHDs

<u>NAME</u>
Total Number:

Names of other research staff

<u>NAME</u>	<u>PERCENT SUPPORTED</u>
FTE Equivalent:	
Total Number:	

Sub Contractors (DD882)

Inventions (DD882)

Final Progress Report
Fundamentals of Wireless Networks: Connectivity
and Capacity
ARO Grant W911NF-06-1-0182

Gerhard Kramer and Yuliy Baryshnikov
Mathematical and Algorithmic Sciences Center
Bell Labs, Alcatel-Lucent
600 Mountain Ave., Murray Hill, NJ 07974

June 9, 2010

Abstract

This report reviews the scientific progress and accomplishments supported by ARO Grant W911NF-06-1-0182: *Fundamentals of Wireless Networks: Connectivity and Capacity*.

1 Introduction

This report reviews the scientific progress and accomplishments supported by ARO Grant W911NF-06-1-0182: *Fundamentals of Wireless Networks: Connectivity and Capacity*.

Results on connectivity center on the cyclic cellular automata model, focussing on the maintaining the topologically connected network of active ad-hoc nodes in a large-scale distributed network.

Results on capacity are based on three main information-theoretic models: wireless network relay channels, cognitive channels, and wire-tap channels.

2 Connectivity

2.1 Introduction

A low-cost, low-energy networks of nodes deployed in large numbers is a characteristic of many proposals relying on the distributed self-organizing, self-adjusting structures aimed at achieving global functions. In our context, the networks are the ad-hoc communication networks, whose function is to maintain uninterrupted flow of information from sources to sinks. One area of applications of high potential is given by the wireless sensor networks (WSN), but the generality of the approaches makes the overall construct rather application agnostic and extremely flexible.

Limited energy is usually accompanied by limited memory, a small computation capability, and a small communication range. To adapt to these constraints, a *sleep-wake protocol* is commonly implemented, whereby the nodes alternate between a low-power sleep mode and a relatively high-power wake mode. The overall system life-time is proportional to the ratio of the total duration of sleep periods to the total duration of active periods, as taken over the duty cycle of this process. A distributed algorithm defined by a local rule coordinates sleep-wake schedules via communications between neighboring nodes within communication range; these communications account for a large part of total energy consumption. Our specific approach focuses on *minimalist self-organizing* techniques, i.e., those making minimal demands on resources, and communication requirements in particular.

In [1, 35], we introduced a class of cellular automata to serve as such a technique. The specific automaton was a generalization of the classical Greenberg-Hastings cyclic cellular automaton on \mathbb{Z}^2 to a continuous, but still synchronous version on \mathbb{R}^2 . In [2], serving as the underlying text for this section, we make a fundamental extension to an asynchronous automaton, which we shall refer to simply as the asynchronous Greenberg-Hastings automaton, or AGHA, and in so doing we eliminate the extensive communication overhead of distributed synchronization algorithms, both in the initialization stage and in re-synchronization stages created by excessive phase drift or by the redeployment of damaged or expired nodes. By means of extensive experimentation, we illustrate both similarities and certain striking changes in behavior relative to the synchronous GHA. We further illustrate refinements of the techniques for designing AGHAs to meet pre-specified modes of behavior. The planting of *seeds*, or artificial nucleating centers, provides the tool for solving these inverse problems of cyclic cellular automata.

The plan of this section is as follows. First, we define GHA and shows how it can be used in sleep-wake scheduling. This presentation

is followed by a brief discussion of relevant background in sleep-wake scheduling. The phase and signaling models are introduced in the next subsection. There we also illustrate the dynamics of the asynchronous Greenberg-Hastings Automaton in \mathbb{R}^2 under these models. Depending on parameters, striking contrasts can be seen in the wave dynamics; explanations of these effects and the basic differences in synchronous and asynchronous wave dynamics are given in the following subsection. Final subsection of this part presents samples of the results of extensive experiments with a focus on the properties of scalability, fault tolerance, effectiveness against intelligent intruders, and seamless accommodation of obstacles in the node field. We conclude by summarizing our findings and by illustrating design of sweep techniques with desirable properties related to intruder detection, forced exit, and entrapment.

2.2 The Greenberg-Hastings Automaton

Each unit square aligned with the regular lattice, is a *cell*(or *site*) in a cellular automaton; cell x has a discrete value, typically an integer, as its state, and a *neighbor set* N_x defining the cells with which x can “communicate.” For example, a commonly studied neighbor set is the von Neumann set consisting of x and the adjacent cells to the north, east, south, and west of x . The state transitions of all cells are synchronized, i.e., they occur at discrete time steps, and they are defined by a universal local rule. Specifically, the transition at cell x at time step t depends on the states of the cells in its neighborhood N_x at time t .

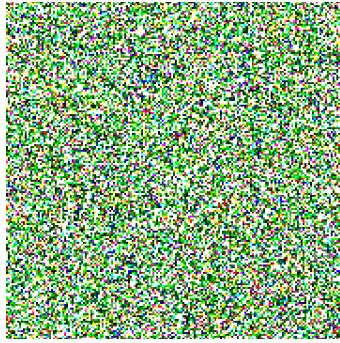
A special class of automata called *cyclic cellular automata* is useful in the design of sleep-wake protocols, and within this class the Greenberg-Hastings Automaton (GHA), defined as follows. Let $\xi_t(x)$ be the state of cell x at time step t .

The state transitions of cell $x \in \mathbb{Z}^2$ in the basic GHA follow the local rule:

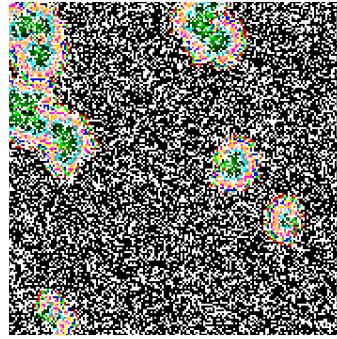
1. If $\xi_t(x) = i > 0$, then $\xi_{t+1}(x) = i + 1 \pmod k$.
2. If $\xi_t(x) = 0$ and at least 1 neighbor in N_x is in state 1, then $\xi_{t+1}(x) = 1$; otherwise, there is no change in state: $\xi_{t+1}(x) = 0$.

The state of a cell is said to be incremented *automatically* if it is nonzero, but only *by contact* if it is 0.

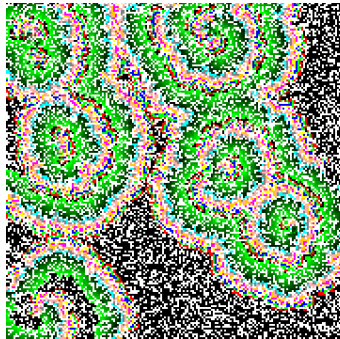
Discretized ad-hoc networks are not normally useful models of actual deployments; instead, the nodes locations should be modeled as points in \mathbb{R}^2 , and in the applications (scales) of interest here, point (cell) locations are reasonably taken as i.i.d. uniform random draws from the deployment terrain, and hence, at the scales of interest here, they will be well approximated by Poisson patterns in two dimensions.



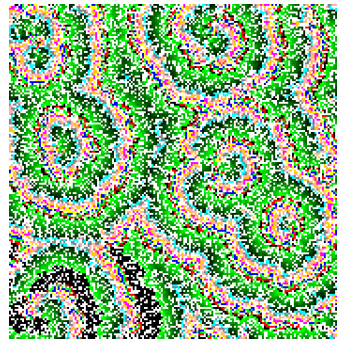
(a) $t = 0$



(b) $t = 10$



(c) $t = 15$



(d) $t = 50$

Figure 1: Greenberg-Hastings Automaton in \mathbb{R}^2 ($k=20$)

Cell x now has a neighborhood N_x defined by all those cells within a disk of given (communication) radius centered at x .

The new GHA model was introduced in [1] and shown to have a periodic behavior very similar to that of the model on \mathbb{Z}^2 . Figure 1 illustrates typical cellular-automata graphics in which states are mapped one-to-one onto colors, and a finite, but large, square represents \mathbb{R}^2 .

Unless stated otherwise, default parameters are unit node density, and respective communication and sensing ranges of $r_c = r_s = 1.5$. Snapshots of the evolution of a GHA with 20 states are shown. Bear in mind the convention: *the color black always denotes state 0*. The initial state is a sample from the uniform product measure on $\{0, \dots, k-1\}$. This is commonly called *primordial soup* with reference to models in biology. Emergent behavior begins by a convergence to state 0 (color black), where the cells stay until they find a neighbor in state 1, an event that will eventually occur by the periodic, expanding circular-shaped figures that originate at groups of cells forming *nucleating centers*. For purposes of mathematical analysis, it is often useful to “close” the finite field by joining opposite edges, passing to the torus as the underlying deployment terrain. This mathematical convenience is bought at a price, however, and we shall just ignore edge effects, as the scale of our experiments and the applications of interest is large enough to make these effects relatively negligible.

Turning to our communication application, point-cells are now relay nodes; state 0 represents the *wake* state in which the node is actively communicating with the active neighbors by passing the messages according to a routing protocol; and state 1 is the state in which the node signals to its small vicinity – essentially, to all nodes within the communication range that it is in state 1, so that those neighbors in state 0 can transition into state 1. States 2 through $k - 1$ are called *sleep* states since no signalling or communication takes place in these states. Figure 2 shows just the nodes in state 0 at $t = 100$ with $k = 12$ and $k = 20$. They form many small, generally curved line segments when $k = 12$ as in Figure 2(a) but they form the closed periodic waves when $k = 20$ as in Figure 2(b). In the appendix Figure 13 helps visualize wave dynamics by giving closely spaced snapshots of the state. Note the important fact that chatter with neighbors, *a high-energy overhead function, can be turned off completely once stable periodic behavior is reached*, which happens quickly for the designs of practical interest.

One critical application of the proposed sleep-wake protocol deals with the wireless sensor networks. With reference to Figure 2(b) consider the occurrence of an event (a fire, appearance of an intruder, ...) at some point of the deployment terrain. It will be detected (i.e., sensed) immediately if it occurs within sensing range of a sensor in state 0. Otherwise, it will be sensed as soon as the next wave of wake sensors gets within sensing range. This may never happen if the wake sensors have large enough gaps between them, but designs where detection is almost certain to happen are easily found by taking the sensor density or sensing range large enough. Of course, if the “event” can move, then it can avoid detection, but eventually it must move out of the sensor field. We cover these details in later sections.

Nucleating centers, i.e., natural seeds, play a key role. If k is cho-

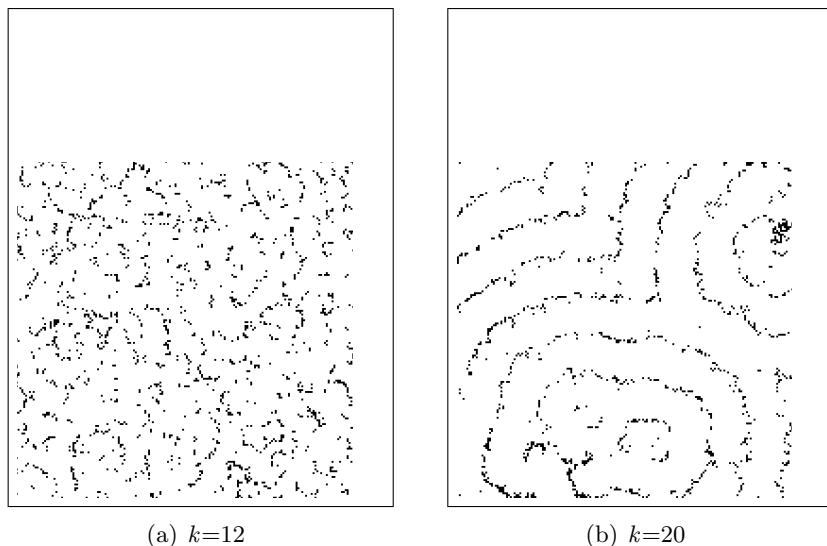


Figure 2: Greenberg-Hastings Automaton in \mathbb{R}^2 ($k = 12, 20$)

sen too large (greater than about 26) then from primordial soup the GHA will *fixate* almost certainly with all nodes permanently in the wake state, i.e., state 0 (the graphic will be all black). In this case there is no natural nucleation in the emergent behavior of the GHA. Classical results show an exponential scaling of the probability of fixation relative to the number, k , of states and the communication area defining neighbor sets. For purposes of the sensor-system application, our interest focuses on values of k that are indeed beyond those for which nucleating centers can be expected to form naturally. In this case, artificial seeds can be planted as a natural, easily implemented extension of the GHA. This technique, introduced in [1], is covered in Section 4 and greatly extended in subsequent sections, especially for intruder entrapment.

Background. The literature dealing with sleep-wake protocols is large, both for synchronous systems [6, 34, 43, 46, 50, 51, 55, 62, 64] and asynchronous [7, 22, 49, 58, 60, 63] systems. These protocols can be classified by general objectives and by the constraints under which they must operate. For example, there exist protocols requiring that link connectivity be preserved [49, 64] and others that require full, or nearly full, coverage of the field at all times [7, 22, 34, 46, 50, 55, 58, 60, 62, 64], and yet others that constrain the delivery of the data to centralized clearing points [6]. The techniques used vary from simple randomization methods [22, 34, 49] to LP-formulations of sleep-schedule optimization [6, 43]

and the domatic partition approach [46, 50]. As is to be expected, the implementation complexity of optimization techniques is substantially, and in applications of interest here, prohibitively greater than that of a minimalist cellular automaton.

Some protocols [60, 63, 64] implement wake-node density control, while others [51] implement "sweep" protocols in much the same spirit as the technique proposed here but much more demanding of resources, i.e., much less of a minimalist protocol for maximizing system lifetime. Wake-node wave-propagation provides a flexible and systematic trade-off between energy consumption and the density of communication active states, and thus the speed of the message propagation.

Many Self organizing schemes were introduced for sleep scheduling. They are similar in that those schemes use distributed algorithm to achieve self organization. However most schemes are different in that they are based on the clustering or they consider full coverage of wake sensors. Note that our scheme is flat protocol and provides partial coverage with guaranteed detection delay. Many references can be found in [3, 8, 16, 23].

2.3 The Asynchronous Greenberg-Hastings Automaton

2.3.1 Phase and Signaling Models

The nodes in the Asynchronous GHA (AGHA) share the same local rule as in the synchronous case; and they are controlled by the same parameters, i.e., the number of states, the communication radius, the cycle length and the node density. We adopt the restricted model of asynchronous systems in which node-clock cycles have constant durations, but differ in their relative phases. We adopt a standard, baseline probability model: The phases of the node clocks are chosen independently and uniformly at random from a discrete set; these sets will be varied and will be stipulated in due course. To keep simulation state spaces small (and experiments not too time-consuming), the size of these sets is kept as small as possible consistent with their purpose, i.e., the size is not taken so small that the properties being studied become unclear or ambiguous.

Compared to synchronous ad-hoc network systems, the nature of the partial overlapping in clock cycles amongst neighbors plays a crucial role in shaping the wake-nodes waves, since successful communication must be made during the overlaps. We propose two different signaling techniques, with different energy requirements, to investigate how clock phase affects the dynamics and performance of an ad-hoc system.

Our first proposed signaling technique is one in which a node in

state 1 broadcasts a signal, a short low-energy burst consistent with the communication range, at both the beginning and end of the clock cycle. This *type-1* clock structure increases the number of communication

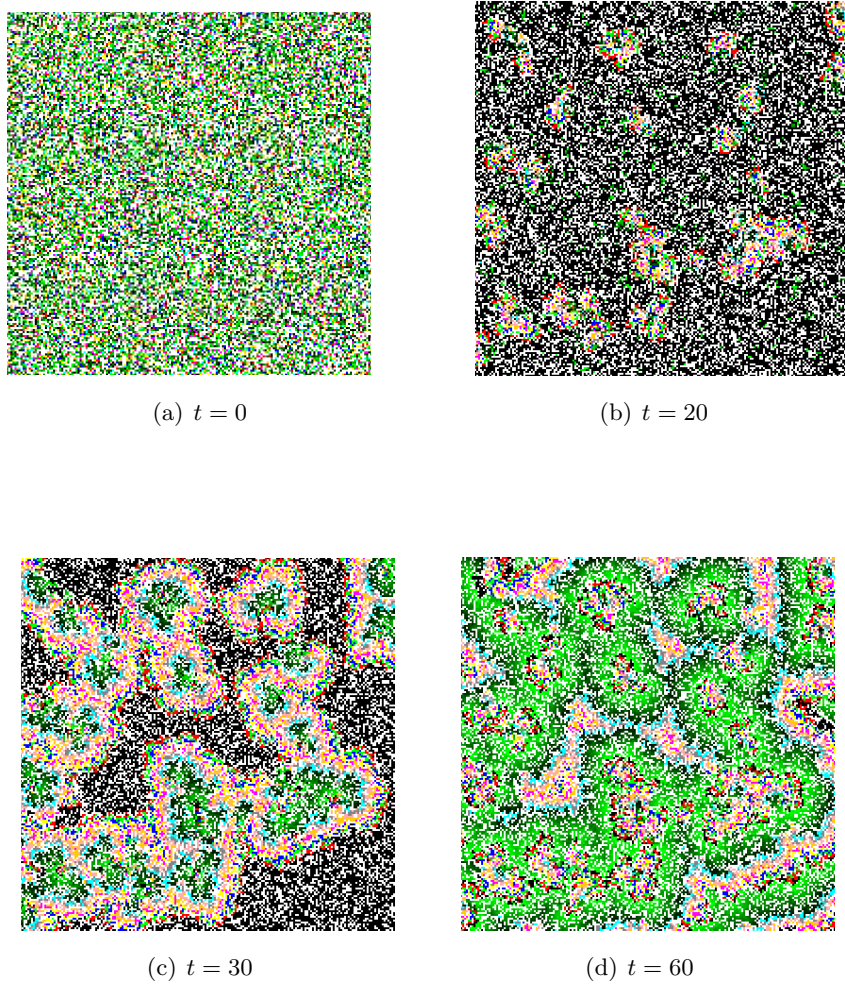


Figure 3: Asynchronous Greenberg-Hastings Automaton in \mathbb{R}^2 ($k=20$)

signals by a factor of two, but it also increases the chance of successful

communication when there are large phase differences; in this sense it is a best-case assumption relative to “catching” a neighbor in state 1, but a worst-case assumption in terms of energy dissipation (in that two signals are used instead of just one).

Our second scheme for comparison is simpler and uses less energy: a node in state 1 broadcasts a signal in the middle of the clock cycle. Adopting this *type-2* scheme decreases the number of communications, keeping signaling at a minimum, but the needed overlap duration becomes larger, i.e., as in the previous section, at least half of a clock cycle must be overlapped to make a successful communication.

2.3.2 Experiments

We begin with a coarse set of possible overlaps: Assume that the phases of the node clocks are chosen so that fractional clock-period overlaps are independently and uniformly distributed on $\{0, 1/5, 2/5, 3/5, 4/5\}$.

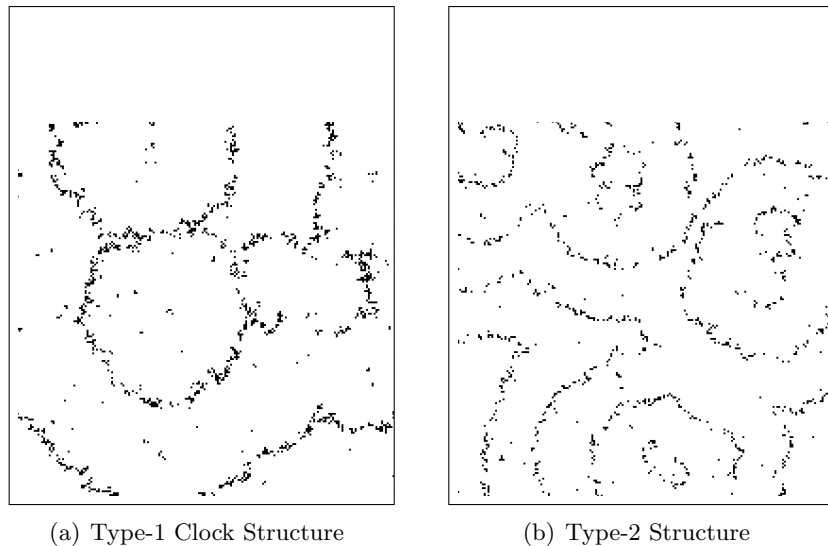


Figure 4: AGHA with Different Clock Structure ($k=20$)

Figure 3 illustrates the sequential evolution of the AGHA with 40,000 nodes placed independently and uniformly at random within a 200×200 field. The process is started in primordial soup with $k = 20$ and $r_c = 1.5$, and type-2 signaling is used. We note that, at this point, there are no striking differences; similar to the (synchronous) GHA, most cells experience a delay in state 0 waiting for a neighbor in state

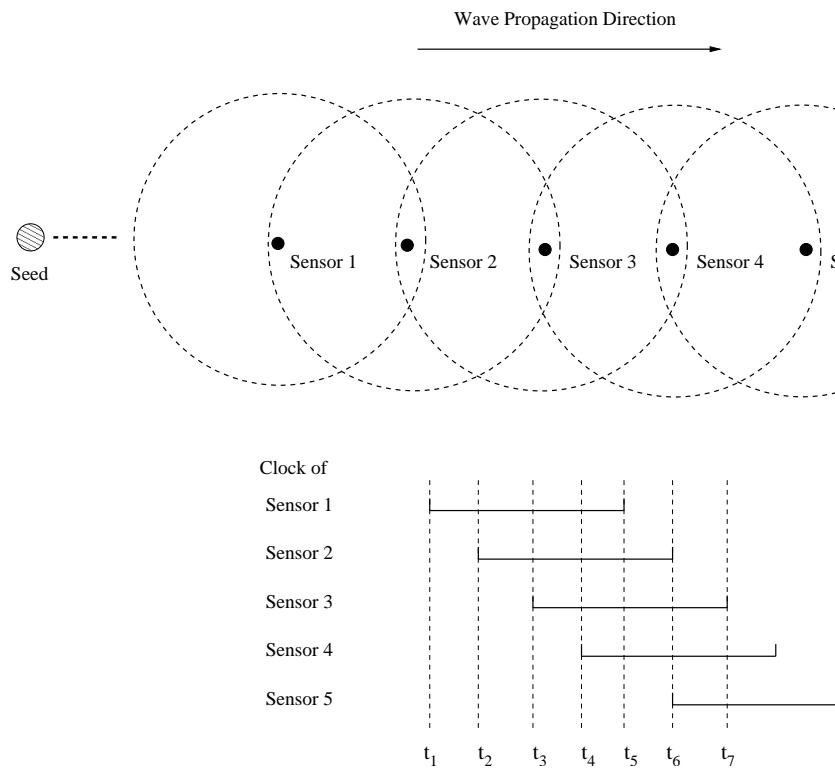


Figure 5: Wake Node Band

1; see Figure 3(b) for an illustration of the asynchronous case. Once a neighbor in state 1 appears, cells start to generate periodic circular wave patterns (or patterns corresponding to the periphery of intersecting circles) just as the synchronous GHA did. see (Figure 3(d)).

Next, consider the type-1 “double” signaling scheme. The snapshot of equilibrium in Figure 4 reveals an interesting property of type-1 signaling: the width of a wake-node band is enlarged, and the gaps

time	1	2	3	4	5
$[t_1, t_2)$	1	0	0	0	0
$[t_2, t_3)$	1	1	0	0	0
$[t_3, t_4)$	1	1	1	0	0
$[t_4, t_5)$	1	1	1	1	0
$[t_5, t_6)$	2	1	1	1	0
$[t_6, t_7)$	2	2	1	1	1
	\vdots	\vdots	\vdots	\vdots	\vdots

Table 1: Node States

between successive waves are correspondingly enlarged. However, as noted earlier the clock-cycle k -periodicity is preserved, as it must be. Thus, the broader wake-node bands propagate faster than in the (synchronous) GHA, so all nodes still come awake every k -th clock cycle. A more detailed explanation of wake-node bands and their variation with parameters is given in the next section. Inspection of Figure 13 shows that the type-2 asynchronous node system differs little from the synchronous case. We also explain this somewhat unexpected phenomenon in the next section.

2.4 Detailed Wave Dynamics

Figure 5 illustrates the conditions under which wide wake-node bands are formed, when we assume type-1 signaling and large k (the system fixates without seeding). The figure considers the nodes in a regular, one dimensional array orthogonal to the direction of wave motion, as this framework greatly simplifies the discussion without obscuring the effects to be brought out. Initially, prior to time t_1 in the figure, all nodes fall into state 0 and wait for a state-1 signal to propagate from a seed. At time t_1 , node 1 responds to a state-1 signal received in the previous clock cycle, increases its state to 1, sends out its first state-1 signal, and remains in state 1 until t_5 . At t_2 , node 2 responds to the state-1 signal from node 1, transitions to state-1, sends out its first state-1 signal and remains in the 1 state until t_6 . This process continues until nodes 1 through 4 are all in state-1 for the last quarter clock cycle of node 1; at this point of the wave dynamic, the width of the wave is created by 4 nodes. The state as a function of time is summarized in Table 1.

For greater widths, we need greater densities, as suggested by Figure 6. Figure 6 illustrates how density affects the widths of wake-node bands. The parameters are $k = 30$, a communication radius of 1.5,

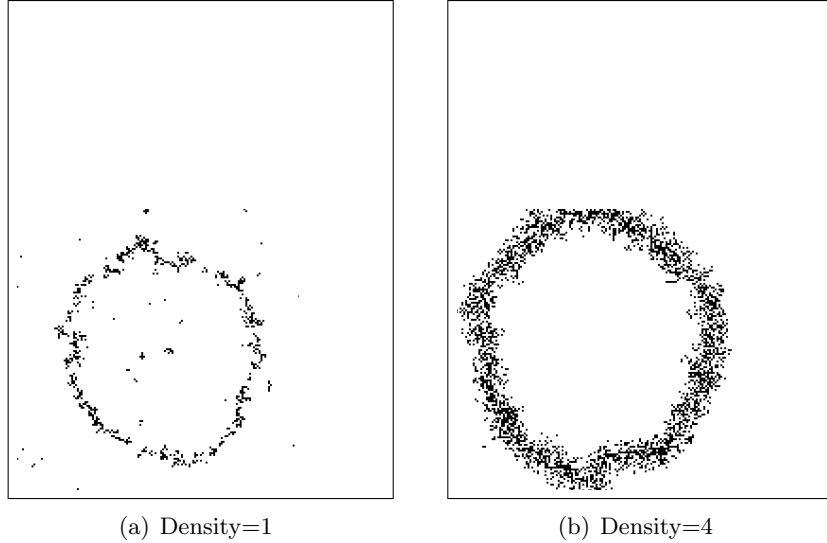


Figure 6: Wake Bands with Different Node Density

nodes are distributed uniformly at random over a 150×150 deployment field, there is a centrally located artificial seed, and initial (fractional) phases are selected uniformly at random from $\{0, 1/40, \dots, 39/40\}$. Results are shown for the node densities 1 and 4. The wavefronts for the higher density are much thicker, as is immediately obvious. The waves are far apart (too far apart to show two of them on the same figure for density 4) and move correspondingly faster in keeping with the local k -periodicity. Interestingly, this method of producing thick and dense wave fronts provides another approach to ensuring high-security blocking of mobile intruders.

Returning to the similarity between the behavior of synchronous and type-2 asynchronous systems, consider the comparison available in Figure 7, where the node field is 150×150 , the density is 2, $k = 30$, $r_c = 1.5$ and there is a single center seed. Phases (fractional overlaps) are multiples of $1/5$. Recall that the synchronous system evolves from primordial soup in three stages: a *reset* stage in which almost all nodes end up in state 0 waiting for a state-1 signal to propagate from the seed, a *stabilization* stage during which the wave dynamics are developed, and finally an *equilibrium* stage in which practically all nodes are effectively independently periodic in a global, deterministic process. For any of the nodes, approximate the number of its neighbors with a phase overlap sufficient for communication by a Poisson random variable with mean given by the product of the density, the commu-

nication area, and the fraction of phases giving sufficient overlap for successful communication between two neighbors: $2 \cdot \pi r_c^2 \cdot 0.6 = 8.482$. Thus, the probability that there are no such neighbors is 2×10^{-4} . As a crude estimate, one can expect the fixation rate to be well below one in a thousand. By our earlier arguments, the thickening of the wave fronts established earlier in this section can be expected to be perceptible for type-2 asynchronous systems only for sufficiently large densities, as in the figure where the density is 2. For densities of 1 or less, the increased width becomes imperceptible. By this informal argument then, one should expect that the synchronous and the type-2 asynchronous wave dynamics will look roughly the same with a small thickening of the wave front for high densities.

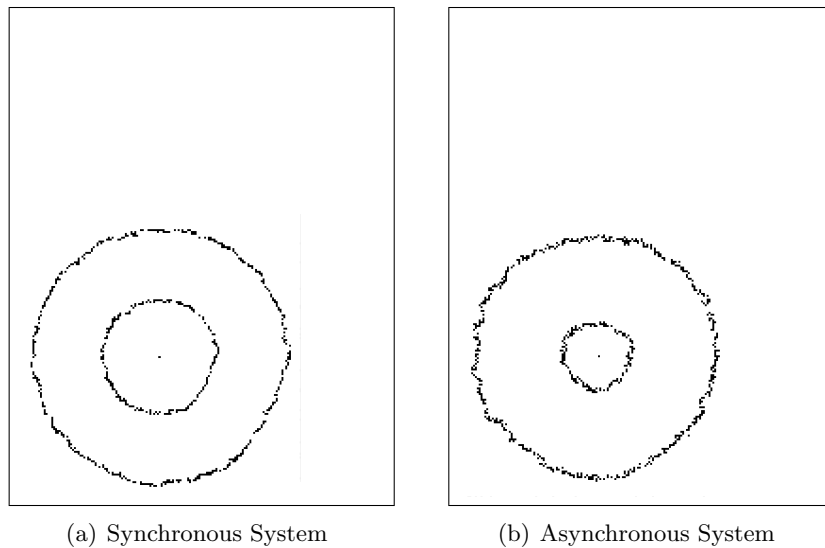
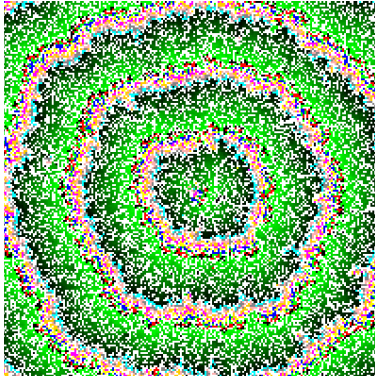
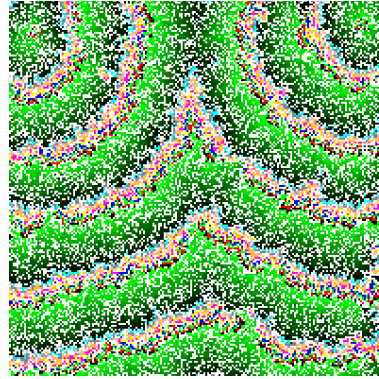


Figure 7: Comparison Between Synchronous and Asynchronous System. (1 single-phase seed at the center of field with $k=30$ and density=2.0.)

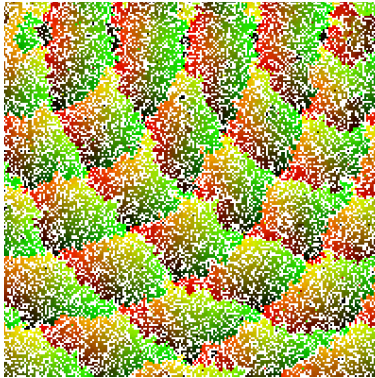
As in the synchronous case, for energy conservation, one prefers large k . The locations of nucleating centers (seeds) will be unpredictable as will be the wake-state wave action they induce, but good performance is assured. Note that fixation is in state 0 so that there will be no sacrifice in surveillance, but the lifetimes of the nodes will be reduced. On the other hand, in the interests of low energy consumption and hence a low duty cycle $1/k$, we will want to take k large. And k does not have to be very large for practical field sizes ($k > 25$ will do when we have density 1, $r_c = 1.5$ and a 100×100 field). *Planting seeds*, i.e., deploying artificial nucleation centers, is a handy and effective so-



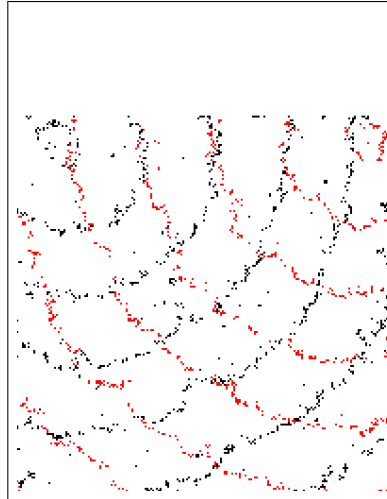
(a) Single-Phase 1 Seed



(b) Single-Phase 2 Seeds



(c) Bi-Phase 2 Seeds



(d) Bi-Phase 2 Seeds: Wake states

Figure 8: Planting artificial seeds with $k=30$

lution for larger k . Any collection of nodes containing a k -cycle serves as a seed. As the term suggests, a k -cycle in the asynchronous node system is a sequence of nodes x_0, \dots, x_{k-1} , who are synchronized each other, such that, for all $k = 0, \dots, k-1$, $\xi_t(x_i) = i$ and $x_{(i+1) \bmod k}$ is in communication range of x_i . Clearly, a k -cycle, which cycles endlessly through the k states, spending one clock period in each state, is trivial

to put together, and renders fixation impossible

Implementations of this technique can be the same as in synchronous system, and performance will remain unchanged except for the wave speed-width details as described above: thicker, faster waves, but with k - periodic equilibria remaining an invariant. Figure 8 illustrates the new but very similar dynamics. Figure 8(a) and 8(b) shows the dynamics of system at time step 200 with $k = 30$ when 1 and 2 artificial seeds with the same state space are planted and function independently.

To enhance connectivity, or to speed up message propoagation, the use of *bi-phase* nodes in a two-seed asynchronous system is a technique worth considering. One obtains results like those in Figure 8(c) and 8(d). Recall that the nodes are now designed to maintain two out-of-phase AGHAs simultaneously, which means a (near) doubling of the wake-node duty cycle.

2.5 Experimental Results

As pointed out earlier, the expected delay, \mathbf{ED} , is the same as in the synchronous case (because of the invariant k -periodicity of a stabilized system). In [1] it is shown that

$$\mathbf{ED} \approx \left(1 - \frac{2r_s}{kr_c}\right) \frac{kr_c - 2r_s}{2r_c}$$

Experiments for the asynchronous system with a center seed gave Table 2, which shows, as in the synchronous case, excellent agreement between the experimental results and the conservative analytical estimate.

We tested the asynchronous system with a stationary link-failure probability p to illustrate how link failures affect system dynamics. Link failure probabilities $p = .1, .3$ are considered in Figure 9. As p

k	Clock Structure 1	Clock Structure 2	Estimates
15	6	7	6
20	8	8	8
25	10	11	11
30	13	13	13
35	16	15	16

Table 2: Estimates of Average Delay (in clock cycles)

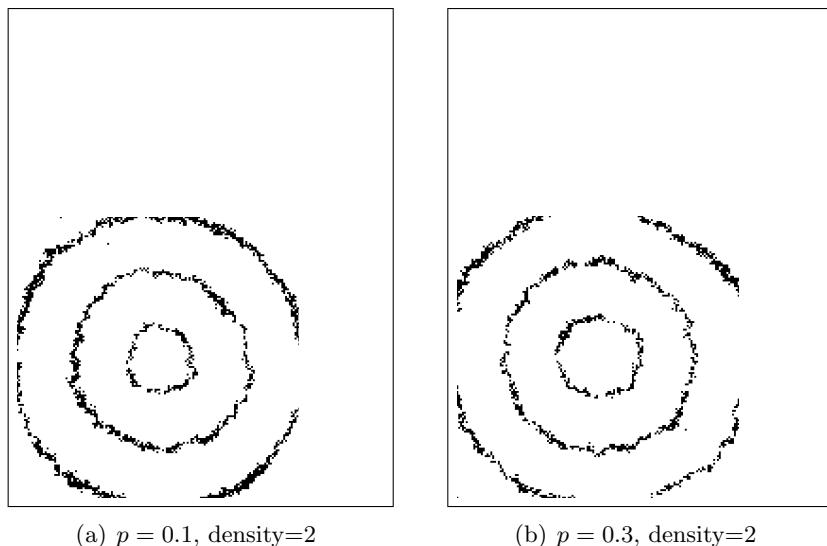


Figure 9: Link Failures in Asynchronous System. (Single seed with $k=30$)

increases, the wake-node wavefronts sustain more “hollows” owing to failures to successfully receive broadcasts from neighboring nodes in state 1. The effects on performance of the AGHA are practically the same as on the GHA, although it should be noted that wake nodes in the AGHA can receive more state-1 signals from neighboring nodes, no matter where the latter are relative to the direction of wave motion; they can be ahead or behind – only the relative phases matter. It is clear from the figures that substantial robustness in the presence of link failures requires substantial node densities.

Seamlessly accommodating obstacles is another property of the GHA that is preserved in the AGHA. To confirm this fact, we again experimented with one big obstacle (40×40) and three small obstacles (20×20) in a 200×200 node field. Figure 10 shows that, as in the synchronous system, our proposed scheme can gracefully work around both the one huge obstacle and the small obstacles; the system continues to pump out periodic waves sweeping the area outside the obstacles; the wake nodes sweep the obstacle along its boundary and close up the waves beyond the obstacle.

As stated earlier, one advantage of the asynchronous system is that nodes can be redeployed without a costly re-synchronization in an area where nodes have expired through damage or old age. The operation of newly deployed nodes is identical to that of nodes in the initial phase. Newly deployed nodes increase their states until they reach state 0 and

wait for a state 1 signal. Once the new nodes receive this signal, they increase their state to 1 and subsequently become a part of the periodic wake-node waves. Figure 11 shows some snapshots of system behavior when nodes are redeployed on a small scale. In the overall field, when it was initialized, 40,000 nodes were deployed in 200×200 field with $k = 40$. One artificial seed is planted at the center of the node field and wake nodes (in state 0) are displayed in black. Figure 11(a) shows the node system as it stabilizes in periodic waves. As illustrated in Figure 11(b), assume certain nodes die (identified as red points with arrows) in two square areas, one in the upper-left and one in the lower-right region of the field. These *inert* areas can be created by external forces such as local flooding, crushing by vehicles, etc. As nodes die, the sensor system adapts itself to the new configuration and begins a self-healing process. Wake node waves sweep along the boundary of the inert areas and keep propagating wake states without major distortions in the dynamics, as in Figure 11(c). To recover the surveillance in the inert areas, new nodes are deployed at random; these eventually reach state 0, and wait for a state-1 signal, as in Figure 11(d). As wake-node waves arrive, new nodes start to catch state-1 signals, coalesce with incoming waves, and knit together a new wave dynamic much like the original. This self-organizing process is complete around 50 clock cycles after redeployment, as shown in Figure 11(f).

This above illustration is typical of small areas of node damage, but as the areas become rather large, the self-organized knitting together of new structures can introduce rather chaotic wave formations, depending on area size and the relative position of the damaged area and the field's artificial seeds. Thus, for larger areas, it is best simply to reset the entire node field, so that it regenerates a regular wave dynamic. This reset control will be part of the centralized re-deployment mechanism

2.6 Conclusion

We have presented a self-organizing, asynchronous sleep-wake protocol for sensor systems that are low-cost, self-healing and long-lived without sacrificing essential properties like fault tolerance and smooth accommodations of obstacles. The method yields an attractive mechanism for trading off system life-time with detection delay. We have shown by comparisons with results in [1] that asynchronous systems are at least as efficient as synchronous ones and have properties, such as wave thickening, that actually improve on performance. By appropriate placement of seeds in systems that otherwise fixate, many different wave patterns may be explored. Against the circular waves of the center-seed system, intruders can not penetrate the field “on the ground” beyond a short distance from the boundaries. An intruder

dropping into the field at any location away from regions near the boundaries is forced to exit staying between consecutive waves if he is to remain undetected.

A state of a total entrapment protocol is illustrated in Figure 12. In the figure, waves are moving up from the bottom and down from the top; while orthogonal waves are moving similarly in a different phase from right to left and left to right. Points of intrusion like the one shown are trapped within a quadrilateral formed by four approaching waves. The intrusion is shown to take place at the center of the field. If it had been chosen off center and the intruder wished to delay entrapment as long as possible, he would have moved toward the center at an appropriate speed, whereupon the same entrapment event would have occurred as shown in the figure.

Appendix 1

Figure 13 gives some idea of wave motion by showing closely spaced snapshots, viz., every 4 time steps; the parameters are those of Figure 1. The emergent behavior can be seen by focusing on the seed locations and watching evolution from the wave nucleations.

3 Capacity

We treat three topics that deal with information-theoretic models:

1. Wireless relaying for half-duplex nodes; results for this topic are half-duplex versions of results in [29, Sec. 4.2].
2. Wireless relaying on lines; results for this topic were developed in the papers [28, 33, 54].
3. Cognitive channels; results for this topic appeared in [40].

The first topic completes results appearing in [29, Sec. 4.2]. The motivation for considering the second channel is to understand the capacity limitations of single-path communication, which is a common form of communication in networks. The third channel allows one to study user cooperation. Our progress for these three areas is reviewed individually below.

3.1 Wireless Relaying Rates for Half-Duplex Nodes

Consider the model of [29, Sec. 4.2] but now with a half duplex relay (see also [29, Sec. 4.3] that treats half-duplex relays from a different perspective). As we will see, the full-duplex and half-duplex cases give basically the same insights.

We begin by reminding the reader of the models used in [29, Sec. 4.2]. The source is node 1, the relay is node 2, the destination is node 3, and the distance between nodes u and v is d_{uv} . The geometry is shown in Fig. 14 where the source and destination nodes are a distance $d_{13} = 1$ apart, and the relay is a distance $d_{12} = |d|$ to the right of the source, and a distance $d_{23} = |1 - d|$ to the left of the destination. A negative d means that the relay is to the left of the source. We remark that we are here considering distances d_{uv} that are less than one, so we are normalizing the source–destination distance to be unity, and including long-range attenuation in the power constraints. We consider channels that exhibit one of three kinds of fading: (1) no fading; (2) fast uniform-phase fading; and (3) fast Rayleigh fading. That is, for every clock tick we have complex channel outputs

$$Y_2 = \frac{H_{12}}{|d|^{\alpha/2}} X_1 + Z_2, \quad (1a)$$

$$Y_3 = H_{13} X_1 + \frac{H_{23}}{|1 - d|^{\alpha/2}} X_2 + Z_3 \quad (1b)$$

where X_1 and X_2 are the source and relay inputs, respectively, Y_2 and Y_3 are the relay and destination channel outputs, respectively, and Z_2 and Z_3 are independent Gaussian random variables with variance N . For no fading, the H_{uv} are constants. For uniform-phase fading,

the H_{uv} are independent and uniform over $\{e^{j\phi} : \phi \in [0, 2\pi)\}$. For Rayleigh fading, the H_{uv} are independent and Gaussian with zero mean and unit variance. The constant α is the attenuation exponent.

We consider the following basic cooperative coding strategies:

1. amplify-and-forward (AF)
2. classic multi-hop
3. compress-and-forward (CF)
4. decode-and-forward (DF).

We consider only strategies where the destination knows ahead of time when the relay is listening or talking, i.e., we ignore the (small) gains of mode modulation, see [29, Sec. 4.3]. However, we do optimize over the amount of time that the relay listens and talks. We consider the attenuation exponent $\alpha = 3$ and choose the power of every node to be $P_1 = P_2 = P_3 = 10$ and the noise variance at every node to be $N = 1$.

3.1.1 No Fading

Suppose there is no fading, i.e., $H_{uv} = 1$ for all u, v . The numerical results are shown in Fig. 15. Not surprisingly, we find that DF is optimal when the relay is near the source, and CF is optimal when the relay is near the destination. Classic multi-hop performs poorly because $\alpha = 3$ is too small. The curve labeled “PDF” gives the rates of a partial-decode-and-forward strategy where the source sends a new message in every block (including the blocks where the relay transmits) and the source and relay do not correlate their transmitted signals. The main point is that PDF can improve on DF.

The curve labeled “coherent AF” shows the rates when the relay listens half the time, and the source repeats its transmissions when the relay talks to permit coherent combining at the receiver. The curve labeled “noncoherent AF” has the source transmitting a new independent message while the relay talks. The relay transmit power was optimized for both cases. Observe the “peaky” behavior of the DF, CF, and classic multi-hop curves near $d = 0$ and $d = 1$.

3.1.2 Phase Fading

Suppose now that there is phase fading, i.e., the H_{uv} are independent and uniform over $\{e^{j\phi} : \phi \in [0, 2\pi)\}$. The rates of PDF, CF, and classic multi-hop do not change. However, we see from Fig. 16 that the DF rates (first solid red curve) drop below that of PDF (solid magenta curve) and that DF, PDF, or CF (second solid red curve) are optimal when the relay is near the source. Otherwise, the insights from the no-fading case remain the same.

3.1.3 Rayleigh Fading

Consider next Rayleigh fading, i.e., the H_{uv} are independent and Gaussian with zero mean and unit variance. For simplicity, we choose the fraction of time the relay listens and transmits to be $1/2$. The resulting rates are shown in Fig. 17. Again, the results are consistent with what we have observed for phase fading above. Perhaps the only surprise is that non-coherent AF performs very well when the relay is near the destination (but recall that we have constrained the relay to listen and transmit half the time).

3.2 Wireless Relaying on Lines

The following model applies to wireless problems in the common situation where every node has a dedicated tone and/or time slot for transmission. If nodes use the same tone at the same time then one should modify the model to include the effects of interference.

Consider a line network with node capacity constraints and broadcasting as shown in Fig. 18. “Supernode” u , $u = 1, 2, 3, 4$, consists of two nodes ui , uo where the “ i ” represents “input” and “ o ” represents “output”. Node uo of supernode u transmits over a broadcast channel (BC) $P(y_{u-1}, y_{u+1}|x_u)$ to nodes $(u-1)i$ and $(u+1)i$ of supernodes $u-1$ and $u+1$, respectively. The BC outputs at node ui of supernode u are thus

$$Y_{u-1,u} = f_{u-1,u}(X_{u-1}, Z_{u-1}) \quad (2)$$

$$Y_{u+1,u} = f_{u+1,u}(X_{u+1}, Z_{u+1}) \quad (3)$$

for some functions $f_{u-1,u}(\cdot)$ and $f_{u+1,u}(\cdot)$, and where the Z_u , $u = 1, 2, \dots, N$, are statistically independent of each other and the X_u . We permit the noise random variables Z_u to be common to $Y_{u,u-1}$ and $Y_{u,u+1}$; this lets us treat any type of memoryless BC. The X'_u in Fig. 18 represent the bits transmitted through supernode u , and we require that $H(X'_u) \leq C_u$ where $H(X)$ is the entropy of X .

For N supernodes $u = 1, 2, \dots, N$, let

$$u \rightarrow \{D\}(u) = \{v(1), v(2), \dots, v(L)\} \quad (4)$$

denote a multicast traffic session, where the $v(1), \dots, v(L)$ are supernodes. The meaning is that a source message is available at supernode u and is destined for supernodes in the set $\{D\}(u)$. We associate sources with input nodes labeled ui and sinks with output nodes labeled uo .

An achievable rate region for these line networks was established in [33] by building on the capacity results of [54], and this work is reviewed below. Summarizing, it was shown in [33] that if all BCs are

either orthogonal or physically degraded, then a “butterfly” binary linear network code achieves capacity and progressive d -separating edge-cut (PdE) bounds [30,31] provide the converse. We further extend the capacity results of [33] to both deterministic and broadcast erasure line networks. The line network defined by (2)-(3) is said to be *deterministic* if Z_u is a constant for all u . The line network is said to be *broadcast erasure* if $Z_u = (Z_{u,u-1}, Z_{u,u+1})$ has alphabet $\{0, 1\} \times \{0, 1\}$ for all u , and $f_{u,u-1}(x, (0, z_{u,u+1})) = f_{u,u+1}(x, (z_{u,u-1}, 0)) = x$ and $f_{u,u-1}(x, (1, z_{u,u+1})) = f_{u,u+1}(x, (z_{u,u-1}, 1)) = \Delta$ where Δ is an erasure symbol.

3.2.1 Traffic Sessions

We use notation from [33]. Let $m(u \rightarrow \{D\}(u))$ and $R(u \rightarrow \{D\}(u))$ denote the message bits and rate, respectively, of traffic session $u \rightarrow \{D\}(u)$. Consider node u . We collect the bits traversing node u 's edge into six sets:

$$m_{LR}^{(u)} = \{m(i \rightarrow \{D\}(i)) : 1 \leq i \leq u-1, \{D\}(i) \cap \{u+1, \dots, N\} \neq \emptyset\} \quad (5)$$

$$m_{RL}^{(u)} = \{m(i \rightarrow \{D\}(i)) : u+1 \leq i \leq N, \{D\}(i) \cap \{1, \dots, u-1\} \neq \emptyset\} \quad (6)$$

$$m_{u,LR} = \{m(u \rightarrow \{D\}(u)) : \{D\}(u) \cap \{1, \dots, u-1\} \neq \emptyset, \{D\}(u) \cap \{u+1, \dots, n\} \neq \emptyset\} \quad (7)$$

$$m_{u,R} = \{m(u \rightarrow \{D\}(u)) : \{D\}(u) \cap \{1, \dots, u-1\} = \emptyset, \{D\}(u) \cap \{u+1, \dots, n\} \neq \emptyset\} \quad (8)$$

$$m_{u,L} = \{m(u \rightarrow \{D\}(u)) : \{D\}(u) \cap \{1, \dots, u-1\} \neq \emptyset, \{D\}(u) \cap \{u+1, \dots, n\} = \emptyset\} \quad (9)$$

$$m_u = \{m(i \rightarrow \{D\}(i)) : \{D\}(i) = \{u\}\} \quad (10)$$

The idea is that $m_{LR}^{(u)}$ and $m_{RL}^{(u)}$ represent traffic flowing from left-to-right and right-to-left, respectively, through node u . Similarly, $m_{u,LR}$, $m_{u,R}$, and $m_{u,L}$ represents traffic originating at node u and destined for nodes on both the left and right, right only, and left only, respectively. Finally, m_u represents traffic destined for node u only. The non-negative message rates are denoted $R_{LR}^{(u)}$, $R_{RL}^{(u)}$, $R_{u,LR}$, $R_{u,R}$, $R_{u,L}$, and R_u . We can now write the capacity result from [54] as follows.

Theorem 1 *The capacity region of a line network with N nodes is*

defined by the bounds, for all u ,

$$\max(R_{LR}^{(u)}, R_{RL}^{(u)}) + R_{u,LR} + R_{u,R} + R_{u,L} + R_u \leq C_u \quad (11)$$

$$R_{RL}^{(u)} + R_{u,LR} + R_{u,L} \leq C_{u,u-1} \quad (12)$$

$$R_{LR}^{(u)} + R_{u,LR} + R_{u,R} \leq C_{u,u+1} \quad (13)$$

Remark 1 *The converse in [54] follows by PdE arguments [31] and achievability follows by using rate-splitting, routing, copying, and “butterfly” binary linear network coding.*

3.2.2 Achievable Rates with Broadcast

We separate channel and network coding, which sounds simple enough. However, every BC receiver has side information about some of the messages being transmitted, so we will need the methods of [32]. We further use the theory in [37] to describe our achievable rate region.

We begin by splitting $m_{u,R}$ and $m_{u,L}$ into two parts each, namely the respective $[m'_{u,R}, m''_{u,R}]$ and $[m'_{u,L}, m''_{u,L}]$. The rates of $m'_{u,R}$ and $m''_{u,R}$ are the respective $R'_{u,R}$ and $R''_{u,R}$, and similarly for $R'_{u,L}$ and $R''_{u,L}$. We choose a joint distribution $P_{S_u T_u W_u X_u}(\cdot)$ and generate a codebook of size

$$2^{n(R_{LR}^{(u)} + R_{RL}^{(u)} + R_{u,LR} + R'_{u,R} + R'_{u,L})}$$

with codewords

$$\underline{w}_u \left(m_{LR}^{(u)}, m_{RL}^{(u)}, m_{u,LR}, m'_{u,R}, m'_{u,L} \right)$$

by choosing every letter of every codeword independently using $P_{W_u}(\cdot)$. Next, for every such \underline{w}_u , we choose $2^{n(R''_{u,R} + R_{T_u})}$ codewords \underline{t}_u by choosing the i th letter $t_{u,i}$ of \underline{t}_u via the distribution $P_{T_u|W_u}(\cdot|w_{u,i})$ where $w_{u,i}$ is the i th letter of \underline{w}_u . We label \underline{t}_u with the arguments of \underline{w}_u , $m''_{u,R}$, and a “bin” index from $\{1, 2, \dots, 2^{nR_{T_u}}\}$. Similarly, for every \underline{w}_u we generate $2^{n(R''_{u,L} + R_{S_u})}$ codewords \underline{s}_u generated via $P_{S_u|W_u}(\cdot)$ and label \underline{s}_u with the arguments of \underline{w}_u , $m''_{u,L}$, and a “bin” index from $\{1, 2, \dots, 2^{nR_{S_u}}\}$.

Next, for every six-tuple of messages, the encoder tries to find a pair of bin indices such that $(\underline{w}_u, \underline{t}_u, \underline{s}_u)$ is jointly typical according to one’s favorite flavor of typicality. Using standard typicality arguments (see, e.g., [37]) a typical triple exists with high probability if n is large and

$$R_{S_u} + R_{T_u} > I(S_u; T_u | W_u). \quad (14)$$

Once this triple is found, we transmit a signal \underline{x}_u that is generated via $P_{X_u|S_u T_u W_u}(\cdot)$.

The receivers use joint typicality decoders to recover their messages. They further use their knowledge about some of the messages (side-information). The result is that decoding is reliable if n is large and (see [32, 37])

$$R''_{u,L} + R_{S_u} < I(S_u; Y_{u,u-1}|W) \quad (15)$$

$$R_{RL}^{(u)} + R_{u,LR} + R'_{u,R} + R_{u,L} + R_{S_u} < I(S_u W_u; Y_{u,u-1}) \quad (16)$$

$$R''_{u,R} + R_{T_u} < I(T_u; Y_{u,u+1}|W) \quad (17)$$

$$R_{LR}^{(u)} + R_{u,LR} + R_{u,R} + R'_{u,L} + R_{T_u} < I(T_u W_u; Y_{u,u+1}). \quad (18)$$

Finally, we use Fourier-Motzkin elimination (see [37]) to remove R_{S_u} , R_{T_u} , $R'_{u,L}$, $R'_{u,R}$, $R''_{u,L}$, and $R''_{u,R}$ from the above expressions and obtain the following result.

Theorem 2 *An achievable rate region for a line network with broadcasting and node constraints and with N nodes is given by the bounds, for any choice of $P(s_u, t_u, w_u, x_u)$ and for all u ,*

$$\max(R_{LR}^{(u)}, R_{RL}^{(u)}) + R_{u,LR} + R_{u,R} + R_{u,L} + R_u \leq C_u \quad (19)$$

$$R_{RL}^{(u)} + R_{u,LR} + R_{u,L} \leq I(S_u W_u; Y_{u,u-1}) \quad (20)$$

$$R_{LR}^{(u)} + R_{u,LR} + R_{u,R} \leq I(T_u W_u; Y_{u,u+1}) \quad (21)$$

$$\begin{aligned} R_{RL}^{(u)} + R_{u,LR} + R_{u,R} + R_{u,L} \\ \leq I(S_u W_u; Y_{u,u-1}) + I(T_u; Y_{u,u+1}|W_u) \end{aligned} \quad (22)$$

$$\begin{aligned} R_{LR}^{(u)} + R_{u,LR} + R_{u,R} + R_{u,L} \\ \leq I(T_u W_u; Y_{u,u+1}) + I(S_u; Y_{u,u-1}|W_u) \end{aligned} \quad (23)$$

$$\begin{aligned} R_{RL}^{(u)} + R_{LR}^{(u)} + 2R_{u,LR} + R_{u,R} + R_{u,L} \\ \leq I(S_u W_u; Y_{u,u-1}) + I(T_u W_u; Y_{u,u+1}) - I(S_u; T_u|W_u). \end{aligned} \quad (24)$$

Remark 2 *The bound (19) is the same as (11).*

Remark 3 *The bounds (20)-(24) are similar to the bounds of [37, Theorem 5]. However, a few rates are “missing” here because nodes $u-1$ and $u+1$ know $m_{LR}^{(u)}$ and $m_{RL}^{(u)}$, respectively, when decoding.*

3.2.3 Orthogonal Channels

A BC $P_{Y_1 Y_2 | X}$ is called *orthogonal* if one can write $X = (X_1, X_2)$ and $P_{Y_1 Y_2 | X} = P_{Y_1 | X_1} P_{Y_2 | X_2}$ (see [12, p. 419]). In fact, if all N broadcast channels in Fig. 18 are orthogonal, then we should recover Theorem 1 from Theorem 2.

Let $X_u = (X_{u,u-1}, X_{u,u+1})$. We choose $S_u = X_{u,u-1}$, $T_u = X_{u,u+1}$, $W_u = 0$ and $X_{u,u-1}, X_{u,u+1}$ independent so that (20)-(24) reduce to

$$R_{RL}^{(u)} + R_{u,LR} + R_{u,L} \leq I(X_{u,u-1}; Y_{u,u-1}) \leq C_{u,u-1} \quad (25)$$

$$R_{LR}^{(u)} + R_{u,LR} + R_{u,R} \leq I(X_{u,u+1}; Y_{u,u+1}) \leq C_{u,u+1}. \quad (26)$$

We have equality in the rightmost inequalities in (25) and (26) by optimizing over $X_{u,u-1}$ and $X_{u,u+1}$. The region of Theorem 1 is therefore achievable. The converse follows by using the same steps as in the converse of Theorem 1. Thus, Theorem 2 reduces to Theorem 1, as desired.

3.2.4 Physically Degraded Channels

A BC $P_{Y_1 Y_2 | X}$ is said to be *physically degraded* if either

$$X - Y_1 - Y_2 \quad \text{or} \quad X - Y_2 - Y_1$$

form Markov chains (see [12, p. 422]). Consider Theorem 2 and suppose that $X - Y_{u,u-1} - Y_{u,u+1}$ forms a Markov chain for all u (the direction of degradation can be adjusted either way for any u for the capacity theorem below). We choose $S_u = X_u$, $T_u = 0$ and the bounds (19)-(24) reduce to

$$\max(R_{LR}^{(u)}, R_{RL}^{(u)}) + R_{u,LR} + R_{u,R} + R_{u,L} + R_u \leq C_u \quad (27)$$

$$R_{LR}^{(u)} + R_{u,LR} + R_{u,R} \leq I(W_u; Y_{u,u+1}) \quad (28)$$

$$R_{RL}^{(u)} + R_{u,LR} + R_{u,R} + R_{u,L} \leq I(X_u; Y_{u,u-1}) \quad (29)$$

$$\begin{aligned} R_{LR}^{(u)} + R_{u,LR} + R_{u,R} + R_{u,L} \\ \leq I(W_u; Y_{u,u+1}) + I(X_u; Y_{u,u-1} | W_u) \end{aligned} \quad (30)$$

We prove the following result.

Theorem 3 *The capacity region of a line network with physically degraded BCs is achieved by separating channel and network coding. For example, if $X - Y_{u,u-1} - Y_{u,u+1}$ forms a Markov chain for all u , then the capacity region is defined by (27)-(30) for any choice of $P(w_u, x_u)$ for all u .*

To prove this theorem, we note that the bound (27) is based on an extension of PdE bounds to mixed wireline/wireless networks [30]. The rest of the converse follows by modifying the steps of [17]. Let $\{S\}$ be a subset of the set $\{V\}$ of network supernodes and let $\{S\}^C$ be the complement of $\{S\}$ in $\{V\}$. We define

$$Y_{\{S\},\{T\}} = \{Y_{u,v} : u \in \{S\}, v \in \{T\}\} \quad (31)$$

and $Y_{u,\{S\}} = Y_{\{u\},\{S\}}$ and $Y_{\{S\},u} = Y_{\{S\},\{u\}}$. Let $M_{u,L}$ be the message random variable corresponding to $m_{u,L}$, and similarly for the other messages. The messages are independent and have entropy equal to n times their rate, where n is the number of times we use each BC. Let $M(\{S\})$ be the set of messages originating at nodes in $\{S\}$, and let $M_{u,L}^C$ to be the set of all network messages except for $M_{u,L}$.

For (28), we let $\{S\} = \{1, 2, \dots, u\}$ and

$$\tilde{W}_{u,i} = (M_{u,L}^C, Y_{u,u+1}^{i-1}) \quad (32)$$

where $Y_{u,u+1}^{i-1} = Y_{u,u+1,1}, Y_{u,u+1,2}, \dots, Y_{u,u+1,i-1}$ and the third subscript index denotes time. Fano's inequality [12, p. 38] bounds the rates for reliable communication as

$$\begin{aligned} & n(R_{LR}^{(u)} + R_{u,LR} + R_{u,R}) \\ & \leq I\left(M_{LR}^{(u)} M_{u,LR} M_{u,R}; Y_{\{S\},\{S\}}^n M(\{S\}^C)\right) \\ & = I\left(M_{LR}^{(u)} M_{u,LR} M_{u,R}; Y_{u,u+1}^n | M(\{S\}^C)\right) \\ & = \sum_{i=1}^n I\left(M_{LR}^{(u)} M_{u,LR} M_{u,R}; Y_{u,u+1,i} | M(\{S\}^C) Y_{u,u+1}^{i-1}\right) \\ & \leq \sum_{i=1}^n I\left(M_{u,L}^C Y_{u,u+1}^{i-1}; Y_{u,u+1,i}\right) \\ & = nI\left(\tilde{W}_{u,Q}; Y_{u,u+1,Q} | Q\right) \\ & \leq nI(W_u; Y_{u,u+1}) \end{aligned} \quad (33)$$

where the fourth step follows because

$$I(A; B|C) \leq I(AC; B) \leq I(ACD; BE)$$

for any random variables A, B, C, D, E . The fifth step follows by defining Q to be a *time-sharing* random variable that is uniform over $1, 2, \dots, n$, and the last step follows by defining $W_u = (\tilde{W}_{u,Q}, Q)$ and $Y_{u,u+1} = Y_{u,u+1,Q}$.

Next, consider (29) and let $\{S\} = \{u, u+1, \dots, N\}$. For reliable communication, we bound

$$\begin{aligned}
& n(R_{RL}^{(u)} + R_{u,LR} + R_{u,R} + R_{u,L}) \\
& \leq I\left(M_{RL}^{(u)} M_{u,LR} M_{u,R} M_{u,L}; Y_{\{S\}, \{S\}^C}^n M(\{S\}^C)\right) \\
& = I\left(M_{RL}^{(u)} M_{u,LR} M_{u,R} M_{u,L}; Y_{u,u-1}^n | M(\{S\}^C)\right) \\
& \leq I\left(M(\{S\}); Y_{u,u-1}^n Y_{u,u+1}^n | M(\{S\}^C)\right) \\
& = \sum_{i=1}^n H\left(Y_{u,u-1,i} Y_{u,u+1,i} | Y_{u,u-1}^{i-1} Y_{u,u+1}^{i-1} M(\{S\}^C)\right) \\
& \quad - H\left(Y_{u,u-1,i} Y_{u,u+1,i} | Y_{u,u-1}^{i-1} Y_{u,u+1}^{i-1} M(\{V\})\right) \\
& \leq \sum_{i=1}^n H(Y_{u,u-1,i} Y_{u,u+1,i}) - H(Y_{u,u-1,i} Y_{u,u+1,i} | X_{u,i}) \\
& = nH(Y_{u,u-1,Q} Y_{u,u+1,Q} | Q) - nH(Y_{u,u-1,Q} Y_{u,u+1,Q} | X_{u,Q}) \\
& \leq nI(X_{u,Q}; Y_{u,u-1,Q} Y_{u,u+1,Q}) \\
& = nI(X_u; Y_{u,u-1}) \tag{34}
\end{aligned}$$

where the fourth step follows by Markovity, and the final step follows by defining $X_u = X_{u,Q}$, $Y_{u,u-1} = Y_{u,u-1,Q}$, and by using the Markov chain due to physical degradation.

Finally, for (30) we use (33) and $\{S\} = \{u, u+1, \dots, N\}$ to bound

$$\begin{aligned}
& n(R_{LR}^{(u)} + R_{u,LR} + R_{u,R} + R_{u,L}) \\
& \leq nI(W_u; Y_{u,u+1}) + I\left(M_{u,L}; Y_{\{S\}, \{S\}^C}^n M(\{S\}^C)\right) \tag{35}
\end{aligned}$$

and

$$\begin{aligned}
& I\left(M_{u,L}; Y_{\{S\},\{S\}^C}^n M(\{S\}^C)\right) \\
& \leq I\left(M_{u,L}; Y_{u,u-1}^n Y_{u,u+1}^n M_{u,L}^C\right) \\
& = I\left(M_{u,L}; Y_{u,u-1}^n Y_{u,u+1}^n | M_{u,L}^C\right) \\
& = \sum_{i=1}^n H\left(Y_{u,u-1,i} Y_{u,u+1,i} | Y_{u,u-1}^{i-1} Y_{u,u+1}^{i-1} M_{u,L}^C\right) \\
& \quad - H\left(Y_{u,u-1,i} Y_{u,u+1,i} | Y_{u,u-1}^{i-1} Y_{u,u+1}^{i-1} M(\{V\})\right) \\
& \leq \sum_{i=1}^n H\left(Y_{u,u-1,i} Y_{u,u+1,i} | \tilde{W}_{u,i}\right) \\
& \quad - H\left(Y_{u,u-1,i} Y_{u,u+1,i} | X_{u,i} \tilde{W}_{u,i}\right) \\
& = nI\left(X_{u,Q}; Y_{u,u-1,Q} Y_{u,u+1,Q} | \tilde{W}_{u,Q} Q\right) \\
& \leq nI\left(X_u; Y_{u,u-1} Y_{u,u+1} | W_u\right) \\
& = nI\left(X_u; Y_{u,u-1} | W_u\right) \tag{36}
\end{aligned}$$

where the last step follows by physical degradation. Collecting the bounds (33)-(36) proves Theorem 3.

3.2.5 Physically Degraded Gaussian Channels

The additive white Gaussian noise (AWGN) physically degraded BC has (see [18])

$$Y_{u,u-1} = X_u + Z_{u,u-1} \tag{37}$$

$$Y_{u,u+1} = Y_{u,u-1} + Z'_{u,u+1} \tag{38}$$

where X_u is real with power constraint $\sum_{i=1}^n X_{u,i}^2 \leq nP_u$ for all u , and $Z_{u,u-1}$ and $Z'_{u,u+1}$ are independent Gaussian random variables with variances $N_{u,u-1}$ and $N'_{u,u+1}$, respectively (again, the direction of degradation can be swapped for any u without changing the results conceptually).

The capacity region is given by Theorem 3 and it remains to optimize $P(w_u, x_u)$. The variances of $Y_{u,u-1}$ and $Y_{u,u+1}$ are at most $P_u + N_{u,u-1}$ and $P_u + N_{u,u-1} + N'_{u,u+1}$, respectively, so the maximum entropy theorem (see [12, p. 234]) gives

$$I(W_u; Y_{u,u+1}) \leq \frac{1}{2} \log(2\pi e(P_u + N_{u,u+1})) - h(Y_{u,u+1} | W_u) \tag{39}$$

$$I(X_u; Y_{u,u-1}) \leq \frac{1}{2} \log(1 + P_u/N_{u,u-1}) \tag{40}$$

$$I(X_u; Y_{u,u-1} | W_u) \leq h(Y_{u,u-1} | W_u) - \frac{1}{2} \log(2\pi e N_{u,u-1}) \tag{41}$$

where $N_{u,u+1} = N_{u,u-1} + N'_{u,u+1}$ and $h(Y|W)$ is the differential entropy of Y conditioned on W . Observe that

$$\begin{aligned} \frac{1}{2} \log(2\pi e N_{u,u+1}) &\leq h(Y_{u,u+1}|W_u) \\ &\leq \frac{1}{2} \log(2\pi e(P_u + N_{u,u+1})) \end{aligned} \quad (42)$$

so there is an α_u , $0 \leq \alpha_u \leq 1$, such that

$$h(Y_{u,u+1}|W_u) = \frac{1}{2} \log(2\pi e(\alpha_u P_u + N_{u,u+1})). \quad (43)$$

Furthermore, a conditional version of the entropy power inequality (see [12, p. 496]) gives

$$\begin{aligned} h(Y_{u,u+1}|W_u) &= h(Y_{u,u-1} + Z'_{u,u+1}|W_u) \\ &\geq \frac{1}{2} \log\left(e^{2h(Y_{u,u-1}|W_u)} + 2\pi e N'_{u,u+1}\right). \end{aligned} \quad (44)$$

Collecting the bounds, and inserting (43) and (44) into (41), we have

$$I(W_u; Y_{u,u+1}) \leq \frac{1}{2} \log\left(1 + \frac{(1 - \alpha_u)P_u}{\alpha_u P_u + N_{u,u+1}}\right) \quad (45)$$

$$I(X_u; Y_{u,u-1}) \leq \frac{1}{2} \log(1 + P_u/N_{u,u-1}) \quad (46)$$

$$I(X_u; Y_{u,u-1}|W_u) \leq \frac{1}{2} \log(1 + \alpha_u P_u/N_{u,u-1}). \quad (47)$$

But we achieve equality in (45)-(47) by choosing

$$X_u = V_u + W_u \quad (48)$$

where V_u and W_u are independent Gaussian random variables with zero-mean and variances $\alpha_u P_u$ and $(1 - \alpha_u)P_u$, respectively. The optimal $P(w_u, x_u)$ is therefore zero-mean Gaussian, and the capacity region is given by inserting (45)-(47) with equality into (28)-(30), and taking the union over the rates permitted by varying α_u .

3.2.6 Discussion

The capacity results in Sec. 3.2.3 and Sec. 3.2.4 imply that one may as well use *decode-and-forward* (DF) relaying, i.e., *amplify-and-forward* (AF) and *compress-and-forward* (CF) do not increase rates (see [29, Ch. 4]). In the next sections, we extend this insight to deterministic and broadcast erasure channels. However, AF and CF strategies are useful for other classes of BCs.

3.2.7 Deterministic Networks

The following theorem gives the capacity of line networks with deterministic BCs.

Theorem 4 *The capacity region of an N -node line network with deterministic BCs and node capacity constraints is given by the union over all choices of $P(w_u, x_u)$, $u = 1, 2, \dots, N$, of the (non-negative) rates satisfying*

$$\max(R_{LR}^{(u)}, R_{RL}^{(u)}) + R_{u,LR} + R_{u,R} + R_{u,L} + R_u \leq C_u \quad (49)$$

$$R_{RL}^{(u)} + R_{u,LR} \leq I(W_u; Y_{u,u-1}) \quad (50)$$

$$R_{LR}^{(u)} + R_{u,LR} \leq I(W_u; Y_{u,u+1}) \quad (51)$$

$$R_{RL}^{(u)} + R_{u,LR} + R_{u,L} \leq H(Y_{u,u-1}) \quad (52)$$

$$R_{LR}^{(u)} + R_{u,LR} + R_{u,R} \leq H(Y_{u,u+1}) \quad (53)$$

$$\begin{aligned} R_{RL}^{(u)} + R_{u,LR} + R_{u,R} + R_{u,L} \\ \leq I(W_u; Y_{u,u-1}) + H(Y_{u,u-1} Y_{u,u+1} | W_u) \end{aligned} \quad (54)$$

$$\begin{aligned} R_{LR}^{(u)} + R_{u,LR} + R_{u,R} + R_{u,L} \\ \leq I(W_u; Y_{u,u+1}) + H(Y_{u,u-1} Y_{u,u+1} | W_u). \end{aligned} \quad (55)$$

A sketch of the proof of this theorem is as follows. Achievability follows by [33, Theorem 2] with $S_u = Y_{u,u-1}$ and $T_u = Y_{u,u+1}$. The methods of [32, 37, 42] are used for broadcasting, and the binary linear network codes of [54] are used to compress data through the nodes. The converse follows in several steps. First, we determine the capacity region of deterministic BCs with message side information by using the methods in [32]. Second, we check that the capacity region of such BCs is not increased by feedback. Third, we adapt the resulting capacity bounds to line networks as was done above or in [33, Sec. IV.B] for physically degraded BCs with feedback [17]. Finally, we apply PdE bounds [30, 31] to include the edge capacity constraint (49).

3.2.8 Broadcast Erasure Networks

Let $\{X\}_u$ be the alphabet of X_u , let $|\{X\}_u|$ be the cardinality of $\{X\}_u$, and let $L_u = \log_2(|\{X\}_u|)$. Suppose that $Z_{u,u-1}$ and $Z_{u,u+1}$ are independent and let $\epsilon_{u,u-1} = \Pr[Z_{u,u-1} = 1]$ and $\epsilon_{u,u+1} = \Pr[Z_{u,u+1} = 1]$ for all u . The following theorem slightly generalizes the main result of [20] and gives the capacity of line networks with broadcast erasure channels.

Theorem 5 *The capacity region of an N -node line network with broadcast erasure channels with independent erasure variables $Z_{u,u-1}$ and*

$Z_{u,u+1}$, $u = 1, 2, \dots, N$, and node capacity constraints is given by the union of the (non-negative) rates satisfying (49) and

$$\frac{R_{RL}^{(u)} + R_{u,LR} + R_{u,L}}{1 - \epsilon_{u,u-1}} + \frac{R_{u,R}}{1 - \epsilon_{u,u-1}\epsilon_{u,u+1}} \leq L_u \quad (56)$$

$$\frac{R_{LR}^{(u)} + R_{u,LR} + R_{u,R}}{1 - \epsilon_{u,u+1}} + \frac{R_{u,L}}{1 - \epsilon_{u,u-1}\epsilon_{u,u+1}} \leq L_u. \quad (57)$$

We sketch a proof of this theorem. Achievability follows by combining the network codes of [20] with the binary linear networks codes of [54]. For the broadcast bounds (56)-(57), we use the same analysis as in [20] except generalized to include message side information. The converse follows by “enhancing” every BC by giving one of the receivers both channel outputs, as is done in [20] and [48]. Next, since every BC is physically degraded, we can apply the same steps as in the proof of [33, Theorem 3] (see Theorem 3 above) to get a collection of outer bounds. Finally, we optimize these bounds over all distributions to obtain (12)-(13). The constraint (49) again follows from PdE bounds.

3.3 Cognitive Channels

Two-sender, two-receiver channel models allow for various forms of transmitter cooperation. When senders are unaware of each other’s messages, we have the interference channel [5, 52]. In wireless networks, however, the broadcast nature of the wireless medium allows nodes to overhear transmissions and possibly decode parts of other users’ messages. An encoder that has such knowledge can use it to improve its own rate as well as the other user’s rate. The level of cooperation and the resulting performance improvement will depend on the amount of information the encoders share, as demonstrated in [13].

Channel models with cooperating nodes are of interest also for networks with cognitive users. Cognitive radio [44] technology is aimed at developing smart radios that are both aware of and adaptive to the environment. Such radios can efficiently sense the spectrum, decode information from detected signals and use that knowledge to improve the system performance. This technology motivates information-theoretic models that try to capture the cognitive radio characteristics. In that vein, we here consider a two-sender, two-receiver channel model in which, somewhat idealistically, we assume that cognitive capabilities allow one user to know the full message of the other encoder, as shown in Fig. 19. The capacity region for this channel is unknown in general, although it has been determined for special cases. No existing coding scheme is known to be uniformly better than other known techniques for all channel characteristics and topologies.

The interference channel with one cooperating encoder was dubbed the *cognitive radio channel* and achievable rates were presented in [13,14]. The capacity region for the strong interference regime in which both receivers can decode both messages was determined in [41]. The capacity region for the Gaussian case of weak interference was determined in [61] and [26]. The results of [26, 61] were extended to the Gaussian MIMO cognitive radio network and shown to achieve the sum-capacity in [53]. The conclusions of [53] apply to the single-antenna cognitive radio channel as well. A general encoding scheme was recently proposed in [24]. Related work can also be found in [4,56]. Scaling laws for cognitive networks were analyzed in [15].

We here present a scheme that generalizes those in [41]- [26]. The scheme is similar to the one in [24]: as in [24] and [13], an encoder uses *rate-splitting* [5] to enable the other receiver to decode part of the interference; the cognitive transmitter cooperates in sending the other user's message to its intended receivers and uses Gel'fand-Pinsker (GP) binning [19] to reduce interference to its own receiver. The key difference of our contribution to the prior work is in the way the binning is performed.

An overview of the encoding scheme is given in the next section. The channel model is described in Section 3.3.3. Details of the encoding scheme are developed in Section 3.3.4. In Section 3.3.6, the encoding scheme is adapted for Gaussian channels and its performance is compared to performance of other coding schemes. Our results demonstrate improvements compared to the general scheme of [24]. In Section 3.3.5, we present two outer bounds for the interference channel with one cooperating encoder. The first bound is based on [47] and the only difference is in the input distribution over which the optimization is performed. We then present an outer bound for the strong interference case that is of the same form as the one in [41, Sec.V] and compare it to the achievable rate region for Gaussian channels.

3.3.1 Overview of the Encoding Strategy

The channel model in Fig. 19 has elements of both the interference channel (IC) and the broadcast channel (BC). Encoding techniques developed for either of these channel models are therefore useful for our model. If the message W_2 of encoder 2 was not known at the cognitive encoder, the channel would reduce to the IC. The best achievable rate region for the IC is achieved by rate-splitting [5, 21]: each encoder divides its message into two parts and encodes each of them with a separate codebook. This allows receivers to decode one of the other user's messages and cancel a part of the interference that it would otherwise create. Rate-splitting was applied to the cognitive radio channel model in [13,24]. In the encoding scheme presented here, rate-

splitting is performed at the cognitive encoder.

The cognitive encoder can employ a number of techniques in addition to rate-splitting. For example, to improve the rate for the noncognitive communicating pair, the cognitive encoder can *cooperate* by encoding W_2 to help convey it to the other decoder. On the other hand, any signal carrying information about W_2 creates interference to the cognitive encoder's receiver. This interference is known at the cognitive transmitter and therefore techniques for precoding against the interference, e.g. GP binning [19] or dirty-paper coding (DPC) [9], can be employed. In fact, GP binning is crucial for the cognitive radio channel: together with cooperation, it achieves capacity in certain scenarios [26, 53, 61]. It is not surprising that DPC brings gains in the Gaussian cognitive radio channel: if the non-cognitive encoder is silent, we have a broadcast channel from the cognitive encoder to the two receivers, for which DPC is the optimal strategy [57, 59].

In general, however, there are two differences at the cognitive encoder from the classical GP setting. First, the interference carries useful information for receiver 2. Second, the interference is a *codebook* of some rate and can thus have lower entropy than in the GP setting. As we will see in Sec. 3.3.2, the latter can be exploited to achieve a higher rate.

We note that due to rate-splitting, there is a common part of W_1 decoded at the both receivers and precoded against interference. Since the signal carrying this common message experiences *different* interference at the two receivers, we use the ideas of [45] and [27] that respectively extend [19] and [9] to channels with different states known non-causally to the encoder. For Gaussian channels, DPC is generalized to *carbon-copying* onto dirty paper [27] to adjust to the interference experienced at both receivers.

Summary of Techniques and Special Cases

Based on the above discussion, a number of techniques may be applied to exploit the additional knowledge of the cognitive encoder:

- Rate-splitting at encoder 1: to improve R_2 through interference cancelation at decoder 2.
- GP binning and binning against a codebook: to improve R_1 by precoding against interference. This approach also allows decoder 1 to decode message W_2 (or part of it) when R_2 is small, as will be shown in Sec. 3.3.2.
- Carbon-copying onto dirty paper: to improve the rate of the common message sent by the cognitive encoder.
- Cooperation: Encoder 1 contributes to R_2 by encoding W_2 .

A general encoding scheme that combines these techniques is described in Section 3.3.4. While this general encoding scheme may not achieve capacity in all scenarios, there are a number of special cases in the scheme for which a subset of techniques suffice to achieve capacity, as we now describe:

1. Strong interference: both decoders can decode both messages with no rate penalty, so there is no need for either rate-splitting or binning. Superposition coding achieves capacity [41].
2. Cognitive decoder has to decode both messages: again, there is no need for binning. Rate-splitting and superposition coding achieve capacity [25, 38].
3. Weak interference at receiver 2: there is no need for a common part of message W_1 and hence for rate-splitting. DPC and cooperation achieve capacity for Gaussian channels [26, 53, 61].

3.3.2 Rate Improvement due to Binning Against a Codebook

For the communication between the cognitive transmitter and its receiver, a codebook carrying W_2 creates interference. The situation is depicted in Fig. 20, where S plays the role of the codebook of rate R_s interfering with the communication of message W at rate R . While in the GP problem the interference S is generated by a discrete memoryless source, the interference in the cognitive setting is a *codebook* of some rate R_s . The next lemma reflects the fact that when R_s is small, this can be exploited for potential rate gains. We prove this Lemma in [40, Appendix B].

Lemma 1 *For the communication situation of Fig. 20, the rate*

$$R \leq \max_{P_{U|S}, f(\cdot)} \min\{I(X; Y|S), \max\{I(U, S; Y) - R_s, I(U; Y) - I(U; S)\}\} \quad (58)$$

is achievable. For $I(S; U, Y) \leq R_s \leq H(S)$, binning achieves the GP rate given by the second term in (58). For $R_s \leq I(S; U, Y)$, superposition coding achieves the rate given by the first term in (58). The two cases are shown in Fig. 21.

Remark 4 *Rate (58) can be written as*

$$R \leq \max_{P_{U|S}, f(\cdot)} \{I(X, S; Y) - \max\{I(S; Y), \min\{R_s, I(U, Y; S)\}\}\}. \quad (59)$$

From (58) and (59), we observe that $I(S; U, Y) \leq R_s \leq H(S)$ corresponds to the classical GP setting. Potential rate improvement comes for $R_s \leq I(S; U, Y)$. Interestingly, in this case the receiver decodes both indexes (w, j) , thus learning both its message and the interference. A related setting in which both data and the channel state information are communicated to the receiver was analyzed in [10, 11].

In the cognitive setting of Fig. 19, index j carries information about W_2 . The implication is that, when R_s is small, receiver 1 will decode a part (or the whole) of W_2 without having encoder 2 rate-split to send common information in the sense of [5, 21].

Recall that, due to rate-splitting, encoder 1 uses two codebooks to send a common and a private index. We denote these respective codebooks as (U_{1c}^N, U_{1a}^N) . We can distinguish four cases depending on whether the two codebooks are generated through binning or superposition coding with respect to X_2^N :

1. Binning: both (U_{1c}^N, U_{1a}^N) are binned against the codebook X_2^N of the non-cognitive encoder.
2. Superposition coding: codebooks are superimposed on X_2^N .
3. Binning then superposition coding: U_{1c}^N is binned against X_2^N , and U_{1a}^N is superimposed on (X_2^N, U_{1c}^N) .
4. Superposition coding then binning: U_{1c}^N is superimposed on X_2^N ; U_{1a}^N is superimposed on U_{1c}^N and binned against X_2^N .

In the last two cases, decoder 1 can decode W_2 due to superposition coding of U_{1a}^N or U_{1c}^N on X_2^N , as shown in Lemma 1. The setting thus corresponds to the *cognitive radio with degraded message sets*. For this channel model, superposition coding achieves capacity [25, 38]. The last two cases can therefore bring no rate improvement. The achievable rate region is the union of two rate regions achieved by binning or superposition coding. We will derive these regions after formally defining the problem in the next section. We remark that in the above encoding scheme, codebook U_{1a}^N is always superimposed on U_{1c}^N . The other encoding choice would be to use binning for U_{1a}^N against the codebook U_{1c}^N .

Finally, we note that encoder 2 also uses rate-splitting and forms two codebooks (X_{2a}^N, X_{2b}^N) using superposition coding. Encoder 1 bins against both codebooks and does not decode a part of W_2 . Following Lemma 1, the respective rates R_{2a} and R_{2b} could be chosen such that (U_{1a}^N, U_{1c}^N) are binned against one of the two codebooks, but superimposed on the other. That would facilitate decoding a part of W_2 at receiver 1.

3.3.3 Channel Model

Consider a channel with finite input alphabets $\mathcal{X}_1, \mathcal{X}_2$, finite output alphabets $\mathcal{Y}_1, \mathcal{Y}_2$, and a conditional probability distribution $p(y_1, y_2 | x_1, x_2)$, where $(x_1, x_2) \in \mathcal{X}_1 \times \mathcal{X}_2$ are channel inputs and $(y_1, y_2) \in \mathcal{Y}_1 \times \mathcal{Y}_2$ are channel outputs. Each encoder t , $t = 1, 2$, wishes to send a message $W_t \in \{1, \dots, M_t\}$ to decoder t in N channel uses. Message W_2 is also known at encoder 1 (see Fig. 19). The channel is memoryless and time-invariant in the sense that

$$\begin{aligned} & p(y_{1,n}, y_{2,n} | x_1^n, x_2^n, y_1^{n-1}, y_2^{n-1}, \bar{w}) \\ &= p_{Y_1, Y_2 | X_1, X_2}(y_{1,n}, y_{2,n} | x_{1,n}, x_{2,n}) \end{aligned} \quad (60)$$

for all n , where X_1, X_2 and Y_1, Y_2 are random variables representing the respective inputs and outputs, $\bar{w} = [w_1, w_2]$ denotes the messages to be sent, and $x_t^n = [x_{t,1}, \dots, x_{t,n}]$. We will follow the convention of dropping subscripts of probability distributions if the arguments of the distributions are lower case versions of the corresponding random variables.

An (M_1, M_2, N, P_e) code has two encoding functions

$$X_1^N = f_1(W_1, W_2) \quad (61)$$

$$X_2^N = f_2(W_2) \quad (62)$$

two decoding functions

$$\hat{W}_t = g_t(Y_t^N) \quad t = 1, 2 \quad (63)$$

and an error probability

$$P_e = \max\{P_{e,1}, P_{e,2}\} \quad (64)$$

where, for $t = 1, 2$, we have

$$P_{e,t} = \sum_{(w_1, w_2)} \frac{1}{M_1 M_2} P[g_t(\mathbf{Y}_t) \neq w_t | (w_1, w_2) \text{ sent}]. \quad (65)$$

A rate pair (R_1, R_2) is achievable if, for any $\epsilon > 0$, there is an (M_1, M_2, N, P_e) code such that

$$M_t \geq 2^{NR_t}, \quad t = 1, 2, \text{ and } P_e \leq \epsilon.$$

The capacity region of the interference channel with a cooperating encoder is the closure of the set of all achievable rate pairs (R_1, R_2) .

3.3.4 Achievable Rate Region

To obtain an inner bound, we employ rate-splitting. We let

$$R_1 = R_{1a} + R_c \quad (66)$$

$$R_2 = R_{2a} + R_{2b} \quad (67)$$

for nonnegative $R_{1a}, R_c, R_{2a}, R_{2b}$, which we now specify.

In the encoding scheme, encoder 2 uses superposition coding with two codebooks X_{2a}^N, X_{2b}^N . Encoder 1 repeats the steps of encoder 2 and adds binning: it encodes the split message W_1 with two codebooks which are Gel'fand-Pinsker precoded against X_{2a}^N, X_{2b}^N . In particular:

1. Binning against X_{2a}^N, X_{2b}^N is used to create a codebook U_{1c}^N of common rate R_c .
2. Binning against X_{2a}^N, X_{2b}^N conditioned on U_{1c} is used to create a codebook U_{1a}^N with private rate R_{1a} .

The encoding structure is shown in Fig. 22.

We have the following result that we prove in [40, Appendix A].

Theorem 6 (joint decoding) *Rates (66)-(67) are achievable if*

$$R_{1a} \leq I(U_{1a}; Y_1 | U_{1c}, Q) - I(U_{1a}; X_{2a}, X_{2b} | U_{1c}, Q) \quad (68)$$

$$R_1 \leq I(U_{1c}, U_{1a}; Y_1 | Q) - I(U_{1c}, U_{1a}; X_{2a}, X_{2b} | Q) \quad (69)$$

$$R_2 \leq I(X_2; Y_2, U_{1c} | Q) \quad (70)$$

$$R_2 + R_c \leq I(X_2, U_{1c}; Y_2 | Q) \quad (71)$$

$$R_{2b} \leq I(X_{2b}; Y_2, U_{1c} | X_{2a}, Q) \quad (72)$$

$$R_{2b} + R_c \leq I(X_{2b}, U_{1c}; Y_2 | X_{2a}, Q) \quad (73)$$

for some joint distribution that factors as

$$p(q)p(x_{2a}, x_{2b}, u_{1c}, u_{1a}, x_1, x_2 | q)p(y_1, y_2 | x_1, x_2) \quad (74)$$

and for which the right-hand sides of (68)-(69) are nonnegative. Q is a time-sharing random variable.

The following theorem is proved following similar steps as the proof of Thm. 6 and is omitted. Details can be found in [39].

Theorem 7 (sequential decoding) *Rates (66)-(67) are achievable if*

$$R_{1a} \leq I(U_{1a}; Y_1 | U_{1c}, Q) - I(U_{1a}; X_2 | U_{1c}, Q) \quad (75)$$

$$R_c \leq \min\{I(U_{1c}; Y_1 | Q), I(U_{1c}; Y_2, X_{2a} | Q)\} \\ - I(U_{1c}; X_2 | Q) \quad (76)$$

$$R_{2a} \leq I(X_{2a}; Y_2 | Q) \quad (77)$$

$$R_{2b} \leq I(X_{2b}; Y_2, U_{1c} | X_{2a}, Q) \quad (78)$$

for some joint distribution that factors as

$$p(q)p(x_{2a}, x_{2b}, u_{1c}, u_{1a}, x_1, x_2|q)p(y_1, y_2|x_1, x_2)$$

and for which the right-hand sides of (75)-(76) are nonnegative.

Remark 5 The rates of Thm. 6 include the rates of Thm. 7.

Remark 6 Thm. 6 includes the rates of the following schemes:

- The scheme of [61, Thm 3.1]: set $X_{2a} = \emptyset, U_{1c} = \emptyset, X_{2b} = (X_2, U)$ and $U_{1a} = V$ so that (68)-(74) become

$$R_2 \leq I(X_2, U; Y_2) \quad (79)$$

$$R_1 \leq I(V; Y_1) - I(V; X_2, U) \quad (80)$$

for $p(u, x_2)p(v|u, x_2)p(x_1|v)$.

- The scheme of [26, Lemma 4.2]: set $X_{2a} = \emptyset, X_{2b} = X_2, U_{1a} = \emptyset$, and $R_1 = R_c, R_2 = R_{2b}$ so that (68)-(74) become

$$\begin{aligned} R_2 &\leq I(X_2; Y_2|U_{1c}) \\ R_1 &\leq \min\{I(U_{1c}; Y_1), I(U_{1c}; Y_2)\} \end{aligned} \quad (81)$$

for $p(x_2)p(u_{1c})$. The strategy in [26] considers the case when

$$I(U_{1c}; Y_1) \leq I(U_{1c}; Y_2). \quad (82)$$

- Carbon-copy on dirty paper [27]: set $X_{2a} = \emptyset, U_{1a} = \emptyset$.
- For $X_{2a} = \emptyset$, our scheme closely resembles the scheme in [24]. One difference in our scheme is that the two binning steps are not done independently which brings potential improvements. Another difference is in the evaluation of error events.

It is also interesting to compare our scheme to the encoding scheme in [13]. The latter combines rate-splitting at both users, with two-step binning at the cognitive user. Each user sends a private index decoded by its receiver and a common index decoded by both. Again, one difference in our scheme is that two binning steps are not independent. Another is that in our scheme the cognitive encoder cooperates by encoding W_2 .

We next exploit Lemma 1.

An Achievable Rate Region with Superposition Coding

Consider a joint distribution (74) and rate R_2 that satisfies

$$R_2 \leq I(X_2; U_{1c}, Y_1) \quad (83)$$

$$R_2 \leq I(X_2; U_{1a}, Y_1 | U_{1c}). \quad (84)$$

From Lemma 1, we know that under conditions (83) and (84), superposition of U_{1c}^N and U_{1a}^N with X_2^N should be used instead of binning. The encoding scheme of the cognitive encoder reduces to rate-splitting and superposition coding. The scheme and the obtained rates reduce to that of [24, Thm. 5] derived for the cognitive radio with degraded message sets, in which the cognitive decoder needs to decode both messages. No rate-splitting at encoder 2 is needed. The resulting achievable rates (R_1, R_2) satisfy

$$\begin{aligned} R_{1a} &\leq I(X_1; Y_1 | X_2, U_{1c}) \\ R_1 &\leq I(X_1; Y_1 | X_2) \\ R_1 + R_2 &\leq I(X_1, X_2; Y_1) \\ R_c + R_2 &\leq I(U_{1c}, X_2; Y_2) \end{aligned} \quad (85)$$

for some joint input distribution $p(x_2, u_{1c}, x_1)$. After Fourier-Motzkin elimination [36], we obtain the following region.

Theorem 8 [25]. *Achievable rates (R_1, R_2) satisfy*

$$\begin{aligned} R_1 &\leq I(X_1; Y_1 | X_2) \\ R_2 &\leq I(U_{1c}, X_2; Y_2) \\ R_1 + R_2 &\leq I(X_1; Y_1 | X_2, U_{1c}) + I(U_{1c}, X_2; Y_2) \\ R_1 + R_2 &\leq I(X_1, X_2; Y_1) \end{aligned} \quad (86)$$

for some joint input distribution $p(x_2, u_{1c}, x_1)$.

Remark 7 *The above region is the capacity region for the cognitive radio with degraded message sets: the converse follows from [38] where a more general case of confidential messages is analyzed.*

3.3.5 Outer Bounds

We next derive two capacity outer bounds proved in [40, Appendix C].

Theorem 9 *The union of the set of rate pairs (R_1, R_2) satisfying*

$$R_1 \leq I(V, U_1; Y_1) \quad (87)$$

$$R_2 \leq I(V, U_2; Y_2) \quad (88)$$

$$R_1 + R_2 \leq \min\{I(V, U_1; Y_1) + I(U_2; Y_2 | U_1, V), \quad (89)$$

$$I(U_1; Y_1 | U_2, V) + I(V, U_2; Y_2)\} \quad (90)$$

for input distributions $p(v, u_1, u_2, x_1, x_2)$ that factor as

$$p(u_1)p(u_2)p(v|u_1, u_2)p(x_2|u_2)p(x_1|u_1, u_2) \quad (91)$$

is an outer bound to the capacity region.

Remark 8 We observe that (87)-(90) is of the same form as the outer bound for the broadcast channel in [47, Sect. 3]. The difference is the factorization of the input distribution.

Remark 9 One can restrict attention to distributions (91) where X_2 is a function of U_2 and X_1 is a function of (U_1, U_2) . The bounds (87)-(90) can then be written as

$$R_1 \leq I(V, U_1; Y_1) \quad (92)$$

$$R_2 \leq I(V, U_2, X_2; Y_2) \quad (93)$$

$$R_1 + R_2 \leq \min\{I(V, U_1; Y_1) + I(X_1, X_2; Y_2|U_1, V), \quad (94)$$

$$I(X_1; Y_1|X_2, U_2, V) + I(V, U_2, X_2; Y_2)\} \quad (95)$$

From (93) and (95), we obtain the outer bound of [61, Thm. 3.2]:

$$R_1 \leq I(X_1; Y_1|X_2) \quad (96)$$

$$R_2 \leq I(U, X_2; Y_2) \quad (97)$$

$$R_1 + R_2 \leq I(X_1; Y_1|X_2, U) + I(U, X_2; Y_2) \quad (98)$$

where we use the notation $U = [U_2, V]$ and also add (96) as it follows by standard methods. The probability distribution factors as

$$p(u, x_1, x_2)p(y_1, y_2|x_1, x_2). \quad (99)$$

Interestingly, (96)-(99) was shown to be tight under weak interference [61, Def. 2.3] and in particular for Gaussian channels with weak interference [26, 61].

The following theorem, proved in [40, Appendix D], gives a simple capacity outer bound in strong interference.

Theorem 10 For an interference channel with one cooperating encoder satisfying

$$I(X_1; Y_1|X_2) \leq I(X_1; Y_2|X_2) \quad (100)$$

for all input distributions $p(x_1, x_2)$, the set of rate pairs (R_1, R_2) satisfying

$$R_1 \leq I(X_1; Y_1|X_2) \quad (101)$$

$$R_1 + R_2 \leq I(X_1, X_2; Y_2) \quad (102)$$

for all input distributions $p(x_1, x_2)$ is an outer bound to the capacity region.

Remark 10 *The bound (102) reflects the fact that, because decoder 2 experiences strong interference, as given by (100), it can decode W_1 with no rate penalty.*

This bound is evaluated for Gaussian channels in (112).

3.3.6 Gaussian Channel

To illustrate our results more concretely, consider the Gaussian interference channel described by

$$Y_1 = X_1 + aX_2 + Z_1 \quad (103)$$

$$Y_2 = bX_1 + X_2 + Z_2 \quad (104)$$

where $Z_t \sim \mathcal{N}[0, 1]$, $E[X_t^2] \leq P_t$, $t = 1, 2$ and $\mathcal{N}[0, \sigma^2]$ denotes the normal distribution with zero mean and variance σ^2 .

Previous Work: Capacity Results

The capacity region for Gaussian cognitive radio channels (103)-(104) was determined for the case of weak interference, i.e., $b \leq 1$, in [26, 61]. The optimum coding strategy at the cognitive encoder consists of encoding message W_1 via DPC while treating X_2^N as interference, and superposition coding to help convey W_2 to receiver 2. Receiver 1 does not suffer interference due to DPC. Because the interference is weak, receiver 2 does not attempt to decode the unwanted message.

For $b \geq 1$, the interference at receiver 2 is stronger than in the previous case, and it is plausible to expect that decoding W_1 (or a part of it) may be beneficial. In fact, we observe from (103)-(104) that *after* decoding W_2 , decoder 2 has a better observation of X_1 than receiver 1, since $b \geq 1$. Therefore, decoder 2 can decode W_1 . However, the conditions under which decoder 2 can decode W_1 also depend on the encoding/decoding approach. In particular, the capacity is known for the strong interference regime in which both decoders can decode both messages. The considered channel becomes a *compound* multiaccess (MAC) channel consisting of two MAC channels, one to each receiver. The strong interference conditions under which this is optimal were determined in [41] leading to the capacity region. These conditions depend on P_1 and P_2 . For $P_1 = P_2$ they simplify to $b > 1$ and $a > b$. Encoder 1 uses a superposition code

$$X_1 = X_{1c} + \sqrt{\frac{\alpha P_1}{P_2}} X_2 \quad (105)$$

where $X_2 \sim \mathcal{N}[0, P_2]$, $X_{1c} \sim \mathcal{N}[0, \alpha P_1]$ and $0 \leq \alpha \leq 1$. Fig. 23 shows the range of channel gains a and b for which the above capacity results apply. In Fig. 23, we choose $P_1 = P_2$.

When the channel conditions do not allow decoding of both messages at decoder 1, they may still enable decoder 2 to decode W_1 . [26, Lemma. 4.2] considers such a case, assuming superposition coding (105). Decoder 2 sequentially decodes: it first decodes W_1 , subtracts the part of the received signal that carries it, and decodes W_2 in the interference-free channel. The obtained rates are given by (81). The conditions under which this encoding/decoding procedure is optimal are given by (82).

When these conditions are not satisfied, there may be other interesting scenarios for which the presented techniques lead to capacity results. For example, consider the case when $a = 0$ in (103). Then (103)-(104) describe a Z -channel where receiver 1 does not suffer interference and the strong interference conditions of [41] are not satisfied. Suppose that encoder 1 is non-cooperating, aimed to achieve the largest possible R_1 . It follows that $\alpha = 0$ in (105). Consider the case for which capacity is unknown, i.e., conditions (82) are not satisfied:

$$\frac{1}{2} \log(1 + P_1) \geq \frac{1}{2} \log \left(1 + \frac{b^2 P_1}{1 + P_2} \right). \quad (106)$$

For this case, the achievable rates evaluate to

$$\begin{aligned} R_1 &\leq \frac{1}{2} \log(1 + P_1) \\ R_1 + R_2 &\leq \frac{1}{2} \log(1 + b^2 P_1 + P_2). \end{aligned} \quad (107)$$

For Gaussian channels, the outer bound (101)-(102) is given by (112). Due to the above assumption of a non-cooperative cognitive encoder, X_1 and X_2 are independent, and $\rho = 0$ in (112). Therefore, the outer bound (112) coincides with the achievable rates (107), yielding capacity.

As the above discussion illustrates, there are still regimes for which the capacity of Gaussian cognitive channels is unknown. This motivates evaluating the general strategy proposed in Thm. 6. We present such an evaluation next.

Numerical Results

We evaluate the rates of Thm. 6 for the special case $X_{2a} = \emptyset$ and $Q = \emptyset$. The rates of Thm.6 reduce to

$$\begin{aligned} R_{1a} &\leq I(U_{1a}; Y_1 | U_{1c}) - I(U_{1a}; X_2 | U_{1c}) \\ R_1 &\leq I(U_{1c}, U_{1a}; Y_1) - I(U_{1c}, U_{1a}; X_2) \\ R_2 &\leq I(X_2; Y_2, U_{1c}) \\ R_2 + R_c &\leq I(X_2, U_{1c}; Y_2). \end{aligned} \quad (108)$$

To simplify (108), we express the conditional entropies in terms of joint entropies, recall that $R_1 = R_c + R_{1a}$, and apply Fourier-Motzkin elimination to obtain

$$\begin{aligned}
R_1 &\leq I(U_{1c}, U_{1a}; Y_1) - I(U_{1c}, U_{1a}; X_2) \\
R_2 &\leq I(X_2; Y_2, U_{1c}) \\
R_2 &\leq I(X_2, U_{1c}; Y_2) \\
R_1 + R_2 &\leq I(X_2, U_{1c}; Y_2) + I(U_{1a}; Y_1, U_{1c}) \\
&\quad - I(U_{1a}; X_2, U_{1c}). \tag{109}
\end{aligned}$$

It is also interesting to evaluate the rates of Thm. 7 achieved with sequential decoding for $X_{2a} = \emptyset, Q = \emptyset$. This evaluation results in

$$\begin{aligned}
R_{1a} &\leq I(U_{1a}; Y_1 | U_{1c}) - I(U_{1a}; X_2 | U_{1c}) \\
R_c &\leq \min\{I(U_{1c}; Y_1), I(U_{1c}; Y_2)\} - I(U_{1c}; X_2) \\
R_2 &\leq I(X_2; Y_2, U_{1c}). \tag{110}
\end{aligned}$$

Remark 11 When $I(U_{1c}; Y_1) \leq I(U_{1c}; Y_2)$, decoder 2 can decode W_1 . Thus, there is no need to rate split at encoder 1 and we choose $U_{1a} = \emptyset$. It follows from (109) and (110) that for this case the same rates can be achieved by sequential decoding or by joint decoding.

Remark 12 We observe from (110) that R_c , being a common rate, is bounded by the worst channel, as reflected by the $\min\{I(U_{1c}; Y_1), I(U_{1c}; Y_2)\}$ term. If $I(U_{1c}; Y_1) > I(U_{1c}; Y_2)$, transmitting X_{2a} will allow decoder 2 to decode part of W_2 before decoding W_c . It will also serve as an observation when decoding W_c as suggested by the expression $I(U_{1c}; Y_2, X_{2a})$ in (76). This will improve the common rate R_c .

We evaluate region (109) for

$$X_2 \sim \mathcal{N}[0, P_2], X_{1c} \sim \mathcal{N}[0, \alpha\beta P_1], X_{1a} \sim \mathcal{N}[0, \alpha\bar{\beta}P_1]$$

$$\begin{aligned}
U_{1c} &= X_{1c} + \lambda_1 X_2 \\
U_{1a} &= X_{1a} + \lambda_2 X_2 \\
X_1 &= X_{1c} + X_{1a} + \sqrt{\frac{\bar{\alpha}P_1}{P_2}} X_2 \tag{111}
\end{aligned}$$

where $0 \leq \alpha, \beta \leq 1$ and $0 \leq \lambda_1, \lambda_2$. Parameters α and β determine the amount of power that the cognitive user dedicates for cooperation and for sending the common message, respectively.

We compare the region (109) to the outer bound of Thm. 10 which for Gaussian channels is given by the following corollary:

Corollary 1 When $b \geq 1$, any achievable rate pair (R_1, R_2) satisfies

$$\begin{aligned} R_1 &\leq \frac{1}{2} \log(1 + (1 - \rho^2)P_1) \\ R_1 + R_2 &\leq \frac{1}{2} \log(1 + b^2 P_1 + P_2 + 2\rho\sqrt{b^2 P_1 P_2}) \end{aligned} \quad (112)$$

for some ρ , $0 \leq \rho \leq 1$.

Fig. 24 shows the achievable rate region (109) and the outer bound (112) for channel gain values $a^2 = 0.3$, $b^2 = 2$ and equal powers $P_1 = P_2 = 6$. Thm. 6 gives larger rates than those of [24, Thm. 5].

When encoder 2 does not transmit (i.e. $P_2 = 0$), the channel reduces to the BC in which there is only the cooperating encoder communicating to two receivers. Unlike the BC channel rate region, the region for the IC with one cooperating encoder is flat for small values of R_2 , reflecting that a cognitive transmitter does not need to cooperate in this regime. It can instead use its full power to precode and transmit W_1 at the single-user rate as if the second user was not present. On the other hand, at $R_1 = 0$ the cooperating encoder fully helps encoder 2, i.e. $\alpha = 0$ and user 2 benefits from the coherent combining gain as indicated by the rate expression

$$R_{2,max} = \frac{1}{2} \log \left(1 + \left(1 + b\sqrt{\frac{P_1}{P_2}} \right)^2 P_2 \right).$$

The achievable rates are very close to the outer bound, especially for large values of R_2 , in the regime where the cognitive encoder dedicates more of its power to cooperate.

Fig. 25 shows achievable rates for different values of P_2 and fixed P_1 . As P_2 decreases, the performance approaches the rate achieved in the BC with only the cooperating encoder transmitting to the two receivers. Since in the BC encoder 2 is not present, the rate region does not depend on P_2 and is given by the dashed line. Fig. 26 shows the effect of reducing power at the cognitive encoder, keeping P_2 constant. This has a strong impact, drastically reducing R_1 .

For the Gaussian channel, the rates achieved with sequential encoding (110) can be evaluated for the choice of random variables X_2, X_1, U_{1a}, X_{1a} as in (111). U_{1c} carries a common message and is precoded against interference. Since the two channels from encoder 1 to the two receivers experience different interference, the carbon-copy method of [27] can be used. More details on this approach are presented in [39]. Fig. 27 shows the performance of the two decoding schemes which can differ significantly.

3.3.7 Discussion

A comparison of our results with [13] would be an interesting next step. As explained in Sec. 3.3.4, the latter combines rate-splitting at both users, with two-step binning at the cognitive user. One of the differences is that, in our scheme the cognitive encoder cooperates by encoding W_2 . However, it is unclear whether our strategy generalizes the scheme in [13], or whether a combination of the two techniques would achieve higher rates. We also compared the proposed scheme to the outer bound that we developed for the strong interference regime. We further developed a new outer bound that extends the Nair-El Gamal broadcast outer bound. Evaluating this bound for specific channels such as Gaussian channels may give capacity results for special cases.

The cognitive radio channel shares some characteristics of both ICs and BCs. Combining encoding strategies developed for either of the two channel models therefore seems a natural approach. However, the optimality of a particular encoding scheme seems to be in part dictated by the channel conditions: for the Gaussian channel in which decoder 2 experiences weak interference, dirty-paper coding achieves capacity. On the other hand, strong interference conditions may allow the cognitive receiver to decode the message not intended for him and therefore DPC against that message is not needed; superposition coding and rate-splitting achieve capacity. An even simpler scheme suffices when both receivers experience strong interference and can both decode the two messages. Neither DPC nor rate-splitting is needed; superposition coding achieves capacity. The encoding scheme presented here is a combination of rate-splitting, GP binning and superposition coding. We believe that this general encoding scheme may achieve capacity for certain special cases related to the channel or specific encoding/decoding constraints.

References

- [1] Y. M. Baryshnikov, E. G. Coffman, and K. J. Kwak. High performance sleep-wake sensor systems based on cyclic cellular automata. In *Proceedings, IPSN '08*, 2008.
- [2] Yu. Baryshnikov, E. G. Coffman, and K.J. Kwak. Self-organizing sleep-wake sensor systems. In *Second IEEE International Conference on Self-adaptive and Self-organizing Systems (Saso 2008)*, 2009.
- [3] P. K. Biswas and S. Phoha. Self-organizing sensor networks for integrated target surveillance. *IEEE Transactions on Computers*, 55(8):1033–1047, 2006.

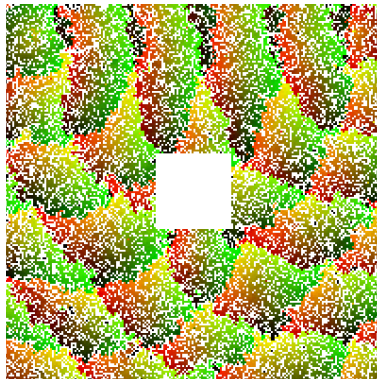
- [4] Y. Cao, B. Chen, and J. Zhang. A new achievable rate region for interference channels with common information. In *Proc. IEEE Wireless Comm. and Networking Conf., Hong Kong*, March 2007.
- [5] A. B. Carleial. Interference channels. *IEEE Trans. Inf. Theory*, 24(1):60–70, January 1978.
- [6] A. Cerpa and D. Estrin. Ascent: Adaptive self-configuring sensor networks topologies. In *Proceedings of IEEE INFOCOM '02*, pages 1278–1287, 2002.
- [7] B. CHen, K. Jamieson, H. Balakrishnan, and R. Morris. Span: An energy-efficient coordination algorithm for topology maintenance in ad hoc wireless networks. *Wireless Networks*, 8(5):481–494, 2002.
- [8] Z. Chen and A. Khokhar. Self organization and energy efficient tdma mac protocol by wake up for wireless sensor networks. In *Proceedings of IEEE SECON '04*, pages 335–341, 2004.
- [9] M. H. M. Costa. Writing on dirty paper. *IEEE Trans. Inf. Theory*, 29(3):439–441, May 1983.
- [10] T. Cover, Y. Kim, and A. Sutivong. Channel capacity and state uncertainty reduction for state-dependent channels. In *Proc. IEEE Int. Symp. Inf. Theory, Nice, France*, June 2007.
- [11] T. Cover, Y. Kim, and A. Sutivong. Simultaneous communication of data and state. <http://arxiv.org/PScache/cs/pdf/0703/0703005v1.pdf>, 2007.
- [12] T. M. Cover and J. A. Thomas. *Elements of Information Theory*. John Wiley & Sons, New York, 1991.
- [13] N. Devroye, P. Mitran, and V. Tarokh. Achievable rates in cognitive radio channels. *IEEE Trans. Inf. Theory*, 52(5):1813–1827, May 2006.
- [14] N. Devroye, P. Mitran, and V. Tarokh. Limits on communications in a cognitive radio channel. In *IEEE Comm. Magazine*, volume 44, pages 44–49, June 2006.
- [15] N. Devroye, M. Vu, and V. Tarokh. Achievable rates and scaling laws for cognitive radio channels. *to appear in EURASIP J. on Wireless Communications and Networking*, February 2008.
- [16] Falko Dressler. *Self-organization in sensor and actor networks*. Wiley, January 2008.
- [17] A. El Gamal. The feedback capacity of degraded broadcast channels. *IEEE Trans. Inf. Theory*, 24(3):379–381, May 1978.
- [18] A. El Gamal. The capacity of the physically degraded gaussian broadcast channel with feedback. *IEEE Trans. Inf. Theory*, 27(4):508–511, July 1981.

- [19] S. I. Gel'fand and M. S. Pinsker. Coding for channel with random parameters. *Problemy Peredachi Informatsii*, 9(1):19–31, 1980.
- [20] L. Georgiadis and L. Tassiulas. Broadcast erasure channel with feedback - capacity and algorithms. In *Network Coding Workshop*, June 2009.
- [21] T. Han and K. Kobayashi. A new achievable rate region for the interference channel. *IEEE Trans. Inf. Theory*, 27(1):49–60, January 1981.
- [22] C. Hua and T. P. Yum. Asynchronous random sleeping for sensor networks. *ACM Transactions on Sensor Networks*, 3(3):15–25, 2007.
- [23] A. Patel J. Degesys, I. Rose and R. Nagpal. Desync: self-organizing desynchronization and tdma on wireless sensor networks. In *Proceedings of ACM/IEEE IPSN '07*, pages 11–20, 2007.
- [24] J. Jiang and Y. Xin. On the achievable rate regions for interference channels with degraded message sets. *IEEE Trans. Inf. Theory*, submitted, April 2007.
- [25] J. Jiang, Y. Xin, and H. Garg. Interference channels with common information. *IEEE Trans. Inf. Theory*, 54(1):171–187, January 2008.
- [26] A. Jovičić and P. Viswanath. Cognitive radio: An information-theoretic perspective. In *Proc. IEEE Int. Symp. Inf. Theory*, pages 2413–2417, July 2006.
- [27] A. Khisti, U. Erez, A. Lapidoth, and G. W. Wornell. Carbon copying onto dirty paper. *IEEE Trans. Inf. Theory*, 53(5):1814–1827, May 2007.
- [28] G. Kramer. Communication on line networks with deterministic or erasure broadcast channels. In *IEEE Inf. Theory Workshop*, October 2009.
- [29] G. Kramer, I. Maric, and R. D. Yates. Cooperative communications. *Foundations and Trends in Networking*, 1(3-4):271–425, 2006.
- [30] G. Kramer and S. A. Savari. Capacity bounds for relay networks. In *Inf. Theory and Appl. Workshop*, February 2006.
- [31] G. Kramer and S. A. Savari. Edge-cut bounds on network coding rates. *Journal of Network and Systems Management*, 14(1):49–67, March 2006.
- [32] G. Kramer and S. Shamai (Shitz). Capacity for classes of broadcast channels with receiver side information. In *IEEE Inf. Theory Workshop*, September 2007.

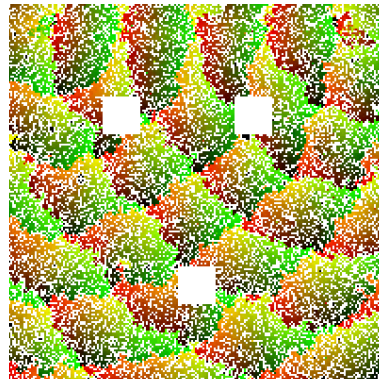
- [33] G. Kramer, S. Tabatabaei-Yazdi, and S. A. Savari. Network coding on line networks with broadcast. In *Conf. on Inf. Sciences and Systems*, March 2008.
- [34] S. Kumar, T. H. Lai, and J. Balogh. On k-coverage in a mostly sleeping sensor network. In *Proceedings of MobiCom' 04*, pages 144–158, 2004.
- [35] Kyung Joon Kwak. *Minimalist Detection and Counting Protocols in Wireless Sensor Networks*. PhD thesis, Columbia University, Electrical Engineering Department, October 2008.
- [36] S. Lall. *Advanced Topics in Computation for Control*. Lecture notes, Stanford University, 2004.
- [37] Y. Liang and G. Kramer. Rate regions for relay broadcast channels. *IEEE Trans. Inf. Theory*, 53(10):3517–3535, October 2007.
- [38] Y. Liang, A. Somekh-Baruch, V. Poor, S. Shamai(Shitz), and S. Verdú. Cognitive interference channels with confidential messages. In *45th Annual Allerton Conference on Communication, Control and Computing, Allerton House, Monticello, IL*, September 2007.
- [39] I. Marić, A. Goldsmith, G. Kramer, and S. Shamai(Shitz). On the capacity of interference channels with a cognitive transmitter. In *Information Theory and Applications (ITA), UCSD, La Jolla, CA* <http://ita.ucsd.edu/workshop/07/files/paper/paper431.pdf>, January 2007.
- [40] I. Maric, A. Goldsmith, G. Kramer, and S. Shamai (Shitz). On the capacity of interference channels with one cooperating transmitter. *Eur. Trans. Telecomms.*, 19(4):405–420, June 2008.
- [41] I. Marić, R. D. Yates, and G. Kramer. Capacity of interference channels with partial transmitter cooperation. *IEEE Trans. Inf. Theory*, 53(10):3536–3548, October 2007.
- [42] K. Marton. A coding theorem for the discrete memoryless broadcast channel. *IEEE Trans. Inf. Theory*, 25(3):306–311, May 1979.
- [43] S. Meguerdichian and M. Potkonjak. Low power 0/1 coverage and scheduling techniques in sensor networks, Jan 2003.
- [44] J. Mitola. *Cognitive Radio Architecture*. John Wiley Sons, Inc., 1991.
- [45] P. Mitran, N. Devroye, and V. Tarokh. On compound channels with side-information at the transmitter. *IEEE Trans. Inf. Theory*, 52(4):1745–1755, April 2006.
- [46] T. Moscibroda and R. Wattenhofer. Maximizing the lifetime of dominating sets. In *Proceedings of the IEEE International Workshop on Algorithms for Wireless, Mobile, Ad Hoc and Sensor Networks*, page 242b, 2005.

- [47] C. Nair and A. El Gamal. An outer bound to the capacity region of the broadcast channel. *IEEE Trans. Inf. Theory*, 53(1):350–355, January 2007.
- [48] L. Ozarow and S. Leung-Yan-Cheong. An achievable region and outer bound for the gaussian broadcast channel with feedback. *IEEE Trans. Inf. Theory*, 30(4):667–671, July 1984.
- [49] V. Paruchuri, S. Basavaraju, R. Kannan, and S. Iyengar. Random asynchronous wakeup protocol for sensor networks. In *Proceedings of IEEE International Conference on Broadband Networks (BROADNETS '04)*, pages 710–717, 2004.
- [50] S. V. Pemmaraju and I. A. Pirwani. Energy conservation via domatic partitions. In *Proceedings of MobiHoc '06*, pages 143–154, 2006.
- [51] S. Ren, Q. Li, H. Wang, X. Chen, and X. Zhang. Design and analysis of sensing scheduling algorithms under partial coverage for object detection in sensor networks. *IEEE Transactions on Parallel and Distributed System*, 18(3):334–350, March 2007.
- [52] H. Sato. Two user communication channels. *IEEE Trans. Inf. Theory*, 23(3):295–304, May 1977.
- [53] Sriram Sridharan and Sriram Vishwanath. On the capacity of a class of MIMO cognitive radios. In *IEEE Information Theory Workshop (ITW 2007), Lake Tahoe, CA*, September 2007.
- [54] S. Tabatabaei-Yazdi, S. A. Savari, and G. Kramer. Network coding capacity region of line networks with node and edge constraints. In *Proc. Allerton Conf. on Commun., Control and Computing*, September 2007.
- [55] D. Tian and N. D. Georganas. A coverage-preserving node scheduling scheme for large wireless snensor networks. In *Proceedings of the 1st ACM International Workshop on Wireless Sensor Networks and Applications (WSNA 02)*, pages 32–41, 2002.
- [56] D. Tuninetti. The interference channels with generalized feedback. In *IEEE Proc. Int. Symp. Inf. Th., Nice, France*, June 2007.
- [57] S. Vishwanath, N. Jindal, and A. Goldsmith. Duality, achievable rates and sum rate capacity of Gaussian MIMO broadcast channels. *IEEE Trans. Inf. Theory*, 49(10):2658–2668, October 2003.
- [58] X. Wang, G. Xing, G. Zhang, C. Lu, R. Pless, and C. Gill. Integrated coverage and connectivity configuration in wireless sensor networks. In *Proceedings of the 1st International Conference on Embedded Networked Sensor Systems (Sensys '03)*, pages 28–39, 2003.

- [59] H. Weingarten, Y. Steinberg, and S. Shamai(Shitz). The capacity region of the Gaussian multiple input multiple output broadcast channel. *IEEE Trans. Inf. Theory*, 52(9):3936–3964, September 2006.
- [60] K. Wu, Y. Gao, and F. Li and Y. Xiao. Lightweight deployment-aware scheduling for wireless sensor networks. *ACM/Kluwer Mobile Networks and Applications (MONET) Special Issue on Energy Constraints and Lifetime Performance in Wireless Sensor Networks*, 10(6):837–852, 2005.
- [61] W. Wu, S. Vishwanath, and A. Arapostathis. Capacity of a class of cognitive radio channels: Interference channels with degraded message sets. *IEEE Trans. Inf. Theory*, 53(11):4391–4399, November 2007.
- [62] T. Yan, T. He, and J. A. Stankovic. Differentiated surveillance service for sensor networks. In *Proceedings of SenSys' 03*, pages 51–62, 2003.
- [63] F. Ye, G. Zhong, J. Cheng, S. Lu, and L Zhang. Peas: A robust energy conserving protocol for long-lived sensor networks. In *Proceedings of the 23rd International Conference on Distributed Computing Systems (ICDCS '03)*, pages 28–37, 2003.
- [64] H. Zhang and J. C. Hou. Maintaining sensing coverage and connectivity in large sensor networks. In *Proceedings of NSF International Workshop on Theoretical and Algorithmic Aspects of Sensor, Ad Hoc Wireless, and Peer-to-Peer Networks, invited paper*, pages 89–124, 2004.



(a) One Obstacle - All nodes



(b) Three Obstacles - All nodes

Figure 10: Working Around Obstacles ($k=30$)

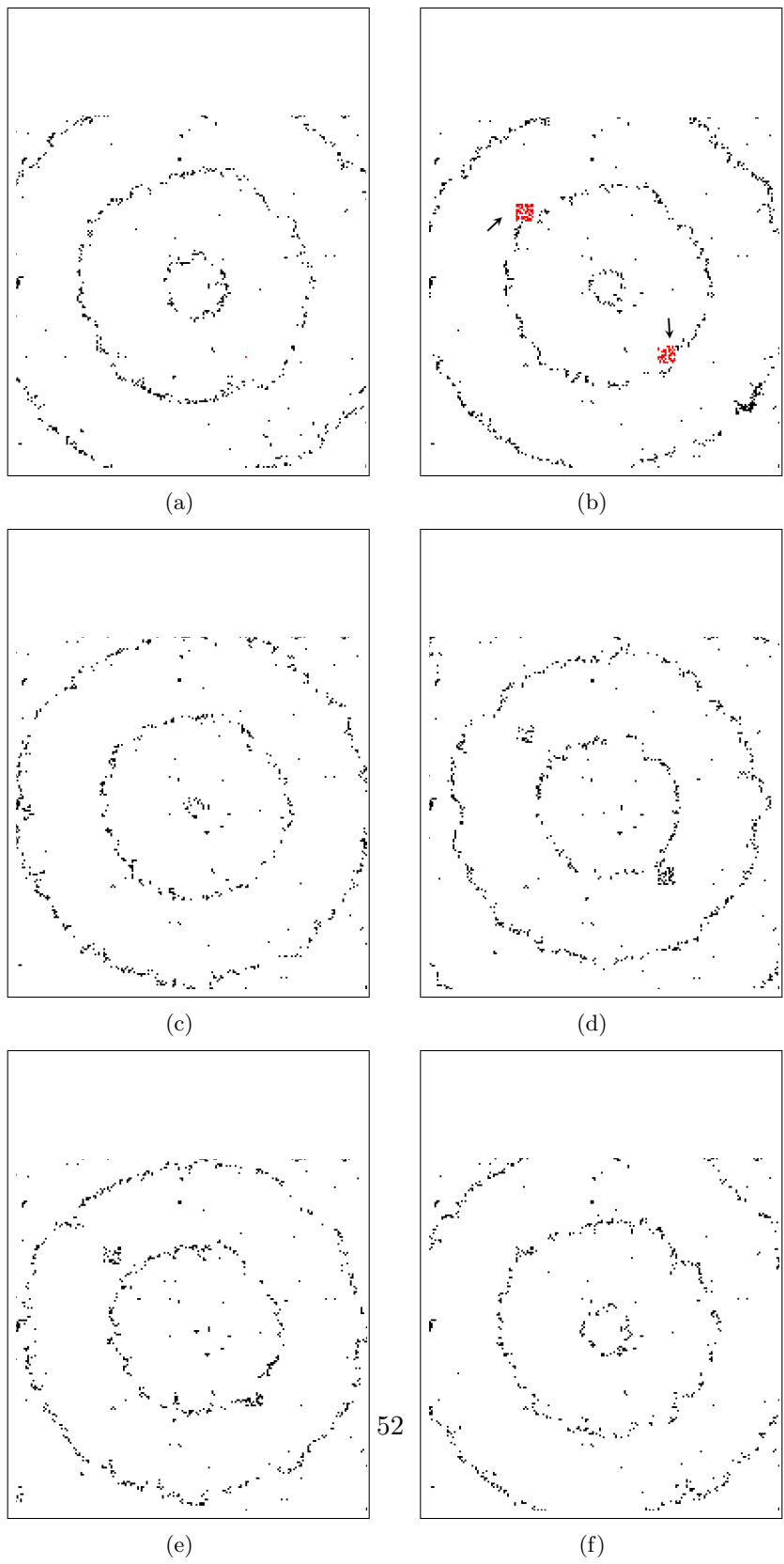


Figure 11: Sensor Redeployment with $k=30$

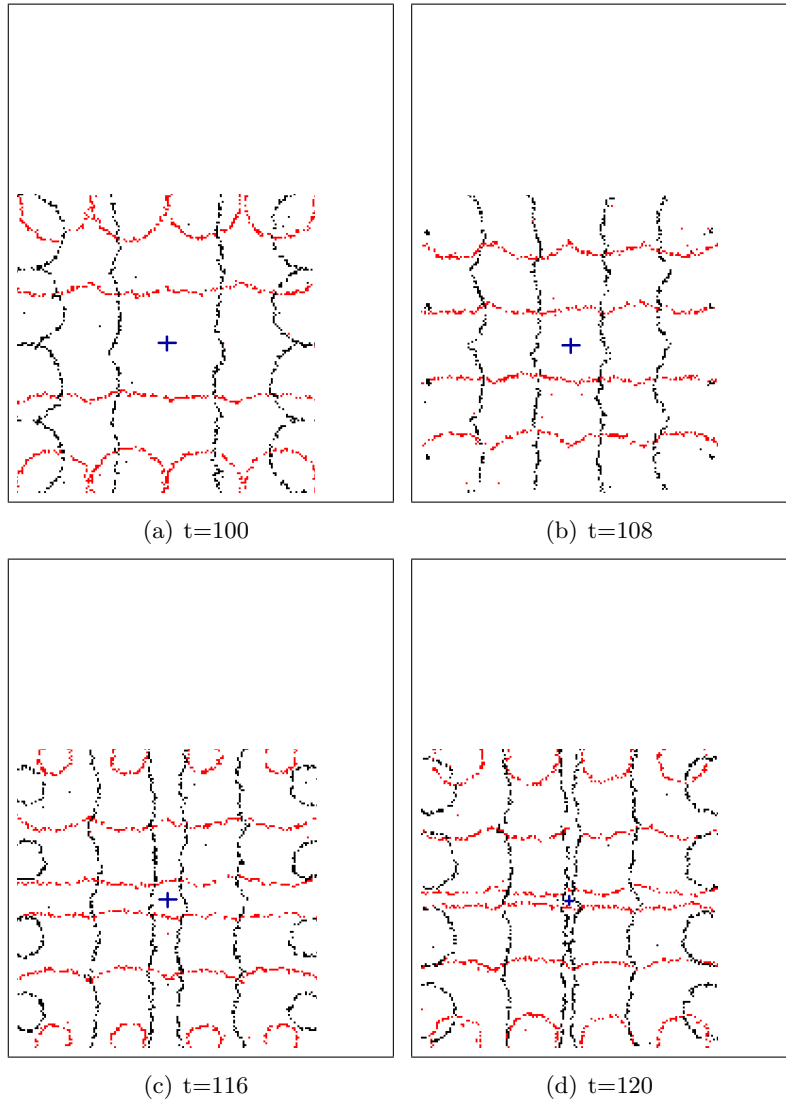
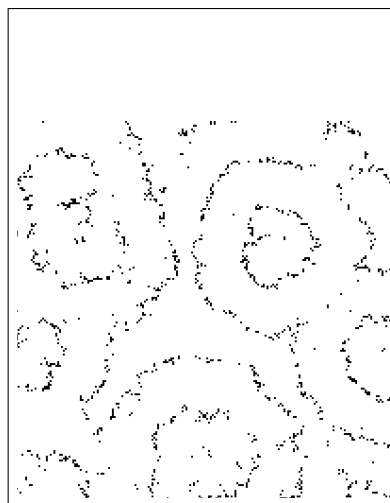
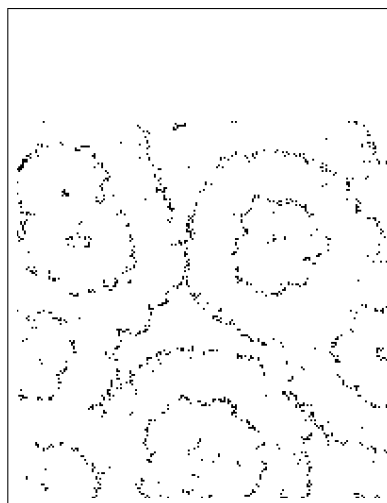


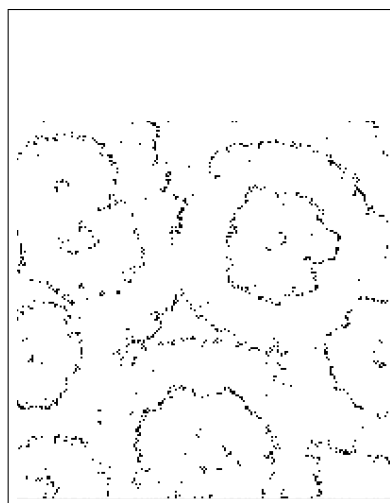
Figure 12: Entrapment: Bi-phase, 8 seeds for each phase, are planted over a 160×160 node field with $k=25$



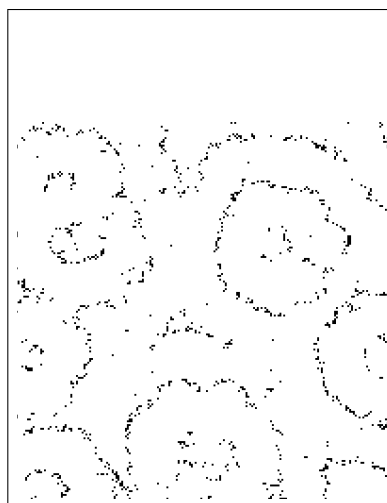
(a) $t = 200$



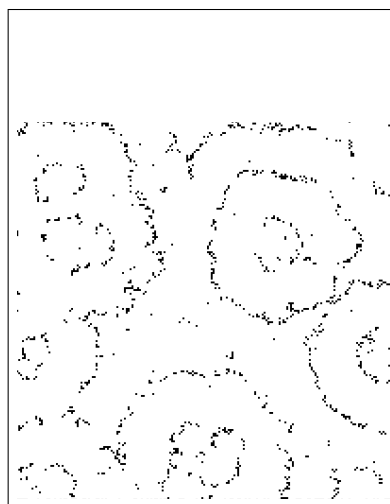
(b) $t = 204$



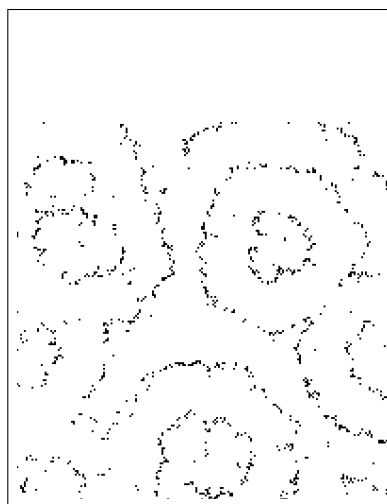
(c) $t = 208$



(d) $t = 212$



(e) $t = 216$



(f) $t = 220$

Figure 13: Greenberg-Hastings Automaton on \mathbb{R}^2 ($k=20$)

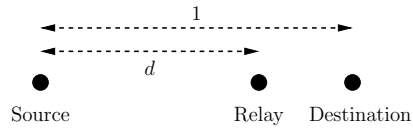


Figure 14: Relay channel geometry.

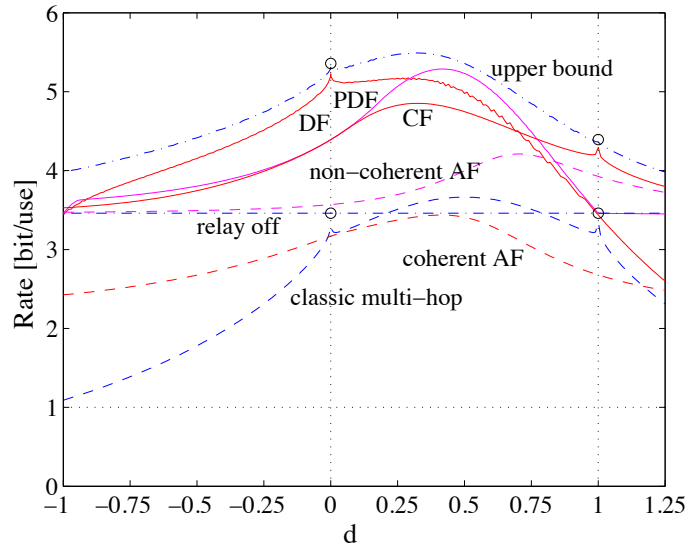


Figure 15: Rates for a half-duplex relay, $P_1/N = P_2/N = 10$, $H_{uv} = 1$ for all (u, v) , and $\alpha = 3$.

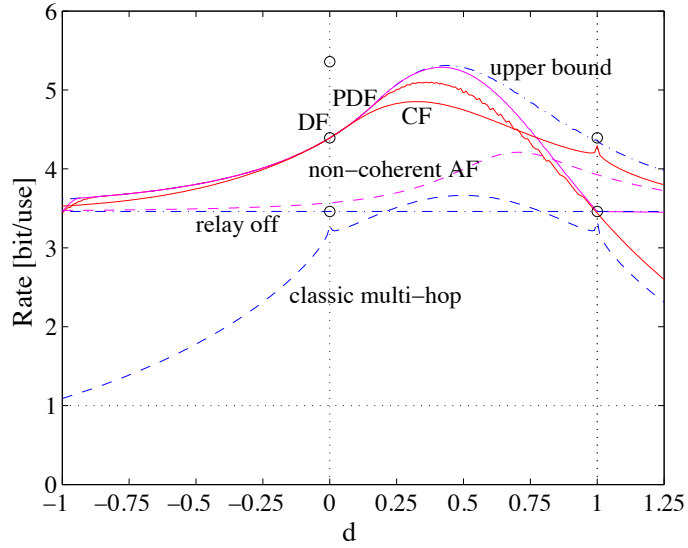


Figure 16: Rates for a half-duplex relay, $P_1/N = P_2/N = 10$, phase fading, and $\alpha = 3$.

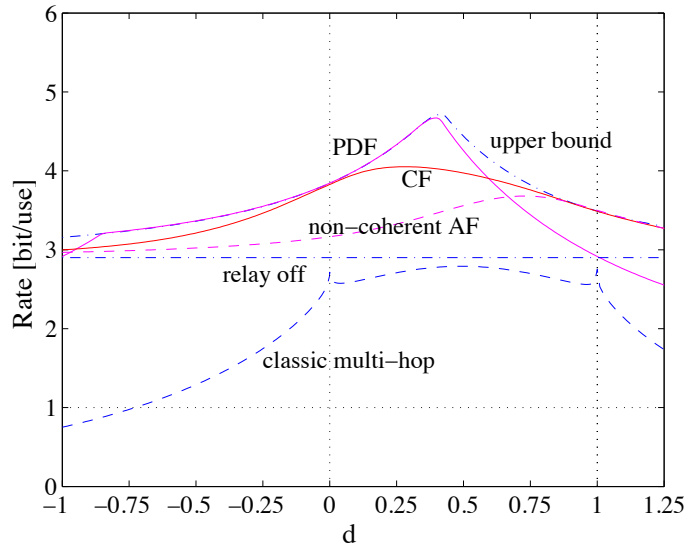


Figure 17: Rates for a half-duplex relay, $P_1/N = P_2/N = 10$, Rayleigh fading, and $\alpha = 3$.

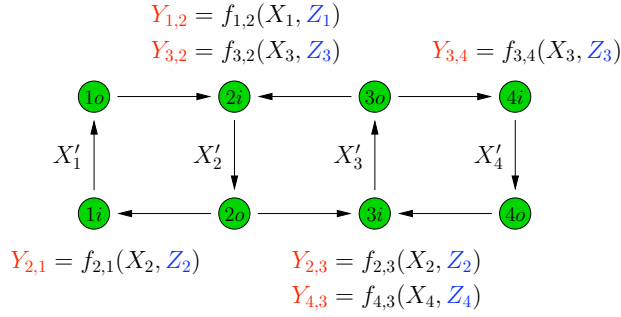


Figure 18: A line network with broadcasting and node capacity constraints.

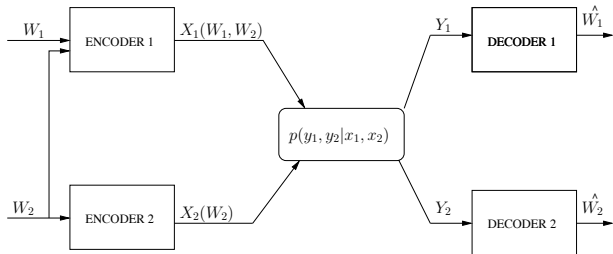


Figure 19: Interference channel with cooperating encoder.

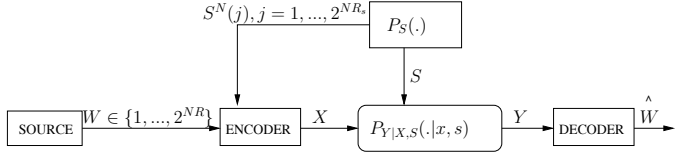


Figure 20: Communication from the cognitive transmitter to its receiver.

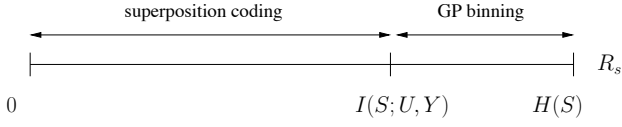


Figure 21: Binning against a codebook.

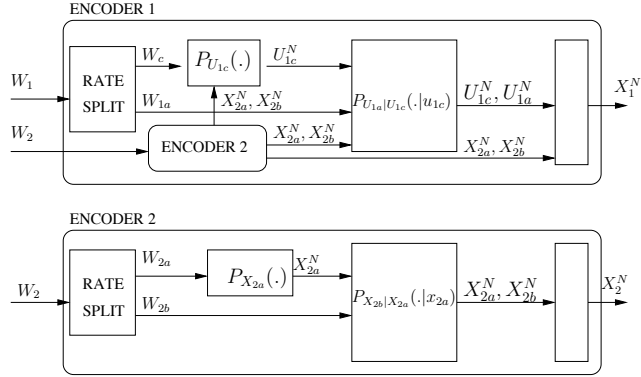


Figure 22: Encoding structure.

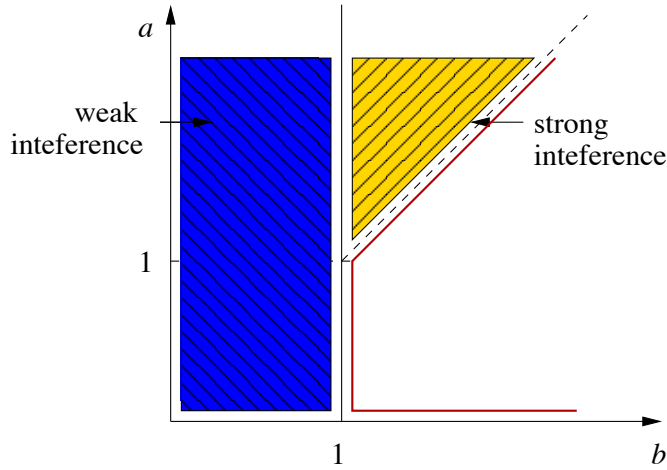


Figure 23: Values of (a, b) for which the capacity region of the Gaussian channel is known. For $b < 1$ the channel has weak interference and the capacity was determined in [26, 61]. Strong interference conditions for case $P_1 = P_2$ are $b > 1$ and $a > b$. The capacity was determined in [41].

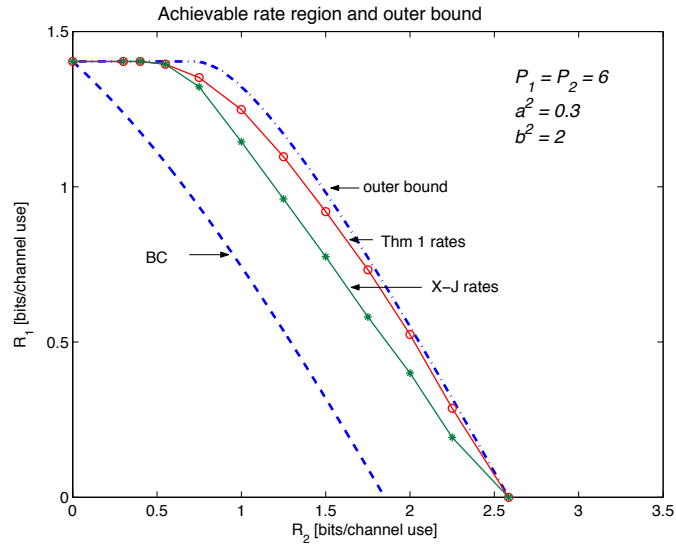


Figure 24: Achievable rates of Thm. 6 and [24, Thm.5] and outer bound of Cor. 1. Also shown is the capacity region of a BC from the cooperative encoder, i.e. the case $P_2 = 0$.

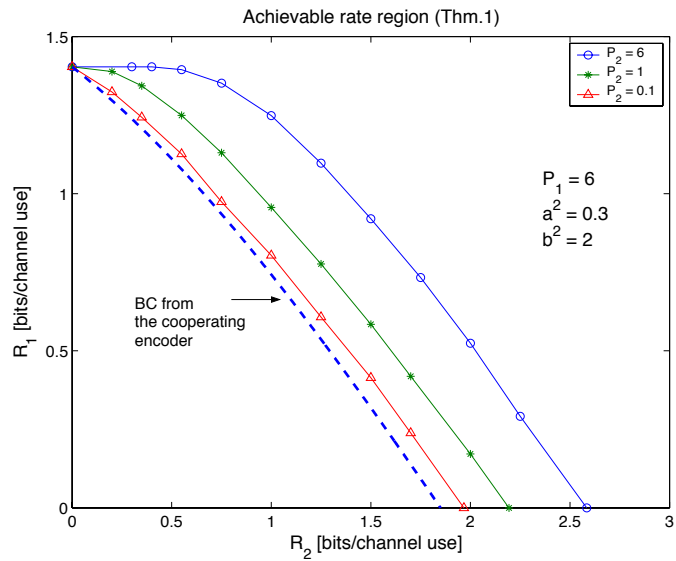


Figure 25: Achievable rates for different values of P_2 .

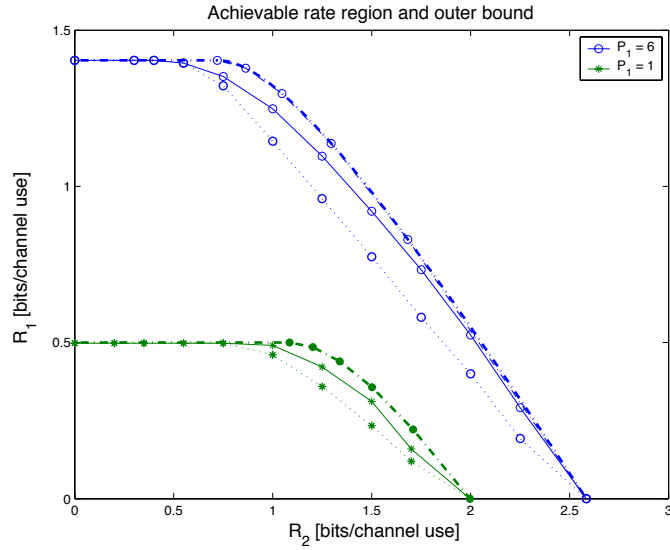


Figure 26: Impact of reduced power of the cognitive transmitter. Rates achieved with Thm. 1 are shown in solid lines and rates of [24] are shown with dotted lines. Dash-dotted lines show the outer bound (112).

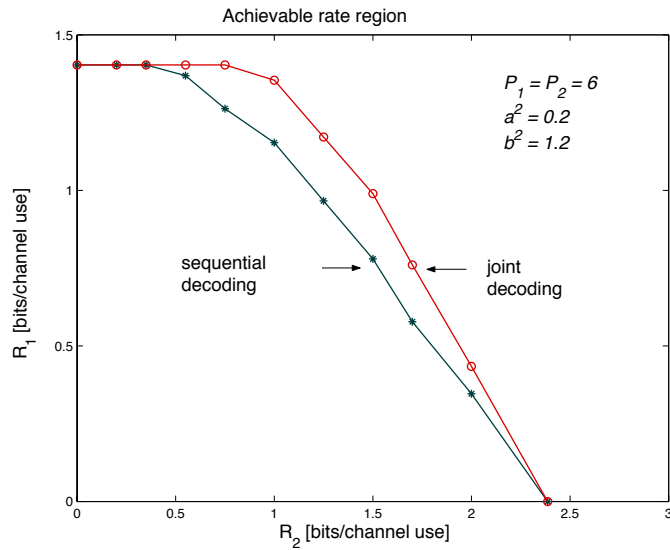


Figure 27: Comparison of achievable rates with joint and sequential decoding.